Biosensors and Bioelectronics: X 27 (2025) 100696

Contents lists available at ScienceDirect

Biosensors and Bioelectronics: X

journal homepage: www.journals.elsevier.com/biosensors-and-bioelectronics-x

Flexible gold nanoparticle SERS tape for rapid, label-free and ultrasensitive detection and differentiation of Shiga toxin variants

A. D'Avino [a,e,1], A. Milano [a,1], V. Marchesano [a,*], B. Guilcapi [a], D. Sagnelli [a], M. Rippa [a], L. Zhou [b], G. Rossi [c], L. Consagra [c], M. Brigotti [c,a], S. Morabito [d,a], L. Petti [a,**]

[a] Institute of Applied Sciences and Intelligent Systems "E. Caianiello" CNR, Pozzuoli, Italy
[b] Shandong First Medical University & Shandong Academy of Medical Sciences, Jinan, China
[c] Dipartimento di Scienze Mediche e Chirurgiche, Sede di Patologia Generale, Università di Bologna, Bologna, Italy
[d] Department of Food Safety, Nutrition and Veterinary Public Health, Istituto Superiore di Sanitá, Rome, Italy
[e] Department of Engineering, University of Naples "Parthenope", Centro Direzionale Isola C4, Napoli, 80143, Italy

ARTICLE INFO

Keywords:
Nanobiosensor
Flexible device
SERS
Shiga toxins
PCA
Biosensing

ABSTRACT

Surface-Enhanced Raman Spectroscopy (SERS) is a highly sensitive technique that enhances Raman signals using plasmonic nanomaterials, enabling the detection of trace biomolecules. Flexible SERS substrates offer advantages such as low cost, adaptability to various surfaces, and reliable performance in complex environments, making them ideal for real-time applications in food safety, environmental monitoring, and diagnostics. In this work, we present a flexible SERS sensor based on Kapton film coated with gold nanoparticles, fabricated through a simple bottom-up method. As a case study, we evaluated, for the first time to the best of our knowledge, its performance in detecting Shiga toxins (Stxs), which are produced by Shiga toxin-producing Escherichia coli (STEC) and are responsible for severe illnesses such as hemorrhagic colitis and hemolytic uremic syndrome. Early and accurate detection of Stxs is critical for outbreak control and timely treatment. We focused on three variants: Shiga toxin 1 (Stx1), Shiga toxin 2 (Stx2), and cleaved Stx2, which are structurally similar but differ in pathogenicity. The SERS spectra collected from each toxin revealed subtle but consistent differences, and Principal Component Analysis (PCA) successfully discriminated between them. Notably, our sensor achieved an outstanding enhancement factor of 7×10^6 and reached an ultra-low limit of detection (LOD) of 15 pM for Stx2 representing, to our knowledge, the lowest LOD reported to date for this toxin using a flexible SERS platform. We also evaluated the LOD in clinically relevant concentrations measured in sera, demonstrating that our system provides a sensitivity suitable for application in real diagnostic settings in the earlier stages of the disease. These results demonstrate the high sensitivity and discriminative power of our sensor, highlighting its strong potential for real-time, on-site monitoring of hazardous biomolecules in fields such as environmental surveillance, food safety, and clinical diagnostics.

1. Introduction

Surface-Enhanced Raman Spectroscopy (SERS) has revolutionized chemical detection, offering ultra-high sensitivity capable of identifying analytes at the single-molecule level (Chen et al., 2015; Lai et al., 2015; Palermo et al., 2021, 2024; Rippa et al., 2022, 2024). Since its discovery, this technique has been widely applied in biosensing, benefiting from advancements in plasmonic nanostructures that enhance signal amplification (Canning et al., 2024; Ditta et al., 2025; Goel et al., 2024; Ilyas et al., 2023; Kadam and Hong, 2022; Ma et al., 2025; Wang et al., 2025; Xie et al., 2025). By precisely engineering nanoparticle properties, including size, shape, and spatial arrangement, SERS can significantly boost local electromagnetic field intensities, enabling the detection of specific toxins at trace concentrations, even within complex biological matrices (Canning et al., 2024; Ditta et al., 2025; Goel et al., 2024; Ilyas et al., 2023; Kadam and Hong, 2022; Ma et al., 2022, 2024, 2025; Wang et al., 2025; Xie et al., 2025). A key advantage of SERS is its label-free detection capability, which eliminates the need for fluorescent or

* Corresponding author.
** Corresponding author.
E-mail addresses: valentina.marchesano@cnr.it (V. Marchesano), lucia.petti@isasi.cnr.it (L. Petti).
[1] The authors contributed equally to the work.

https://doi.org/10.1016/j.biosx.2025.100696
Received 13 June 2025; Received in revised form 25 September 2025; Accepted 3 October 2025
Available online 7 October 2025

enzymatic markers. This simplifies the assay workflow while improving the reproducibility. Moreover, the development of flexible SERS sensors has unlocked new opportunities for real-time, on-site molecular detection, especially in complex and irregular environments. Unlike their rigid counterparts, these sensors leverage soft, adaptable substrates that allow them to conform to uneven surfaces, interact efficiently with analytes, and operate under aqueous conditions. The most employed materials include PDMS (Haque Chowdhury et al., 2023; Li et al., 2022; Liang et al., 2022; Liu et al., 2020; Ma et al., 2022; Pan et al., 2024; Peng et al., 2025; Sun et al., 2023; Tan et al., 2023; H. Zhang et al., 2023; Zhang et al., 2022; Y. Zhang et al., 2023), PVA (Pham et al., 2023; Shao et al., 2024a), PVDF (Chen et al., 2024; J. Wang et al., 2023), paper (Beeram et al., 2022; Jun Dong, 2023; Liu R, 2020; Nguyen et al., 2024; Verma et al., 2022; Yadav et al., 2024; Zhang et al., 2020; X. Zhang et al., 2024; Zhao et al., 2022), polyurethane (Bai et al., 2021), agar (Chang et al., 2022; Picone et al., 2022), graphene (Verma et al., 2022; K. S. Wang et al., 2024; Yu et al., 2022), and biological membranes (H. Wang et al., 2024; Yang et al., 2024; You et al., 2023a; Yu et al., 2023), each chosen for their unique properties. Elastomeric substrates such as PDMS and polyurethane offer stretchability (Bai et al., 2021; Haque Chowdhury et al., 2023; Li et al., 2022; Liang et al., 2022; Liu et al., 2020a; Ma et al., 2022; Pan et al., 2024; Peng et al., 2025; Sun et al., 2023; Tan et al., 2023; H. Zhang et al., 2023; Zhang et al., 2022; Y. Zhang et al., 2023), whereas paper and agar provide biocompatibility and eco-friendliness (Beeram et al., 2022; Chang et al., 2022; Liu R et al., 2020; Jun Dong, 2023; Nguyen et al., 2024; Picone et al., 2022; Verma et al., 2022; Yadav et al., 2024; Zhang et al., 2020; X. Zhang et al., 2024; Zhao et al., 2022). Graphene, on the other hand, enhances plasmonic performance, further boosting detection sensitivity (Verma et al., 2022; K. S. Wang et al., 2024; Yu et al., 2022). One of their major advantages is their low-cost and scalable fabrication. While traditional SERS substrates rely on expensive nanofabrication techniques, flexible materials can be processed using simple and cost-efficient methods, significantly reducing production complexity. Unlike rigid platforms that require careful positioning and controlled sample deposition, flexible SERS sensors naturally conform to the surface to which they are applied. This feature is particularly valuable for applications involving food surfaces, biological tissues, and environmental monitoring, where direct contact with the target sample enhances detection efficiency. Another key advantage of these materials is their compatibility with aqueous environments. Many flexible substrates exhibit hydrophilic properties, which facilitate analyte absorption and retention in liquid samples. This makes them especially suited for water quality assessment, food safety testing, and biomedical applications, where traditional hydrophobic substrates often struggle to retain biomolecules in solution. Moreover, their porous and absorbent nature eliminates the need for time-consuming pre-treatment steps, allowing direct sample application without additional drying, dilution, or chemical modifications. In many cases, this capability enables in situ detection, making flexible sensors an attractive alternative for real-time monitoring and point-of-care diagnostics (Bai et al., 2021; Beeram et al., 2022; Chang et al., 2022; Chen et al., 2024; Haque Chowdhury et al., 2023; Jun Dong, 2023; Li et al., 2022; Liang et al., 2022; Liu et al., 2020a; Ma et al., 2022; Nguyen et al., 2024; Pan et al., 2024; Peng et al., 2025; Pham et al., 2023; Picone et al., 2022; Rongyang et al., 2020; Shao et al., 2024; Sun et al., 2023; Tan et al., 2023; Verma et al., 2022; J. Wang et al., 2023; K. S. Wang et al., 2024; Yadav et al., 2024; Yu et al., 2022; H. Zhang et al., 2023; Zhang et al., 2022, 2020; X. Zhang et al., 2024; Y. Zhang et al., 2023; Zhao et al., 2022).

Among flexible SERS substrates, Kapton has emerged as a promising candidate due to its exceptional thermal stability, chemical resistance, and mechanical flexibility. Developed by DuPont, Kapton is a polyimide film known for maintaining its structural integrity across extreme temperatures, from cryogenic conditions to over 400 °C. Its high electrical insulation properties make it widely used in electronics, aerospace, and flexible sensor technologies. One major advantage of Kapton is its intrinsically low Raman background, which enhances the detection of weak analyte signals. Additionally, its long-term stability against thermal degradation, UV exposure, and harsh chemicals makes it ideal for industrial and field applications requiring durable sensors. Kapton-based flexible sensors are widely utilized across various fields due to their robustness and versatility. In biomedical and wearable devices, they are employed in health monitoring systems to track heart rate, respiration, temperature, and muscle activity. Electronic skin (E-Skin) mimics human skin for robotic and prosthetic applications, while implantable sensors monitor physiological parameters inside the body due to their biocompatibility (Binnwei, n.d.; Pang et al., 2013; Wang et al., 2021). In the aerospace and automotive industries, Kapton-based sensors play a crucial role in structural health monitoring by detecting strain, pressure, and temperature variations in aircraft and spacecraft (Bhattacharya et al., n.d.; Brandon et al., 2011). They are also essential in flexible circuitry for aerospace electronics, where lightweight and flexible materials are required, and in automotive sensors integrated into smart vehicle dashboards and driver monitoring systems (Srinivasan et al., 2023). For industrial and environmental monitoring, these sensors are used in high-temperature industrial processes such as temperature and pressure sensors (Lahokallio et al., 2014; Martiny et al., 2014; Phan et al., 2020). They also function as gas and chemical sensors, detecting toxic gases and pollutants in industrial safety systems (Ramezani Farani et al., 2024; Rezaei et al., 2024). Additionally, smart textiles incorporate these sensors (Ataman et al., 2013) for real-time environmental sensing. In robotics and human-machine interaction (Ataman et al., 2013), tactile sensors enable soft robotics to detect touch, pressure, and motion, enhancing their adaptability. Haptic feedback devices further improve user interaction in virtual and augmented reality applications. The combination of durability, stability, and low Raman background makes Kapton a key material for next-generation flexible sensing technologies, particularly in challenging environments where precision and reliability are critical (Madani et al., 2024; McDonnell et al., 2023a; Prakash et al., 2019; Seifi et al., 2022). Despite their potential, current research on flexible SERS sensors has primarily focused on pesticide detection, particularly thiram (Bai et al., 2021; Chen et al., 2024; Jun Dong, 2023; Liang et al., 2022; Liu et al., 2020a; Ma et al., 2022; Peng et al., 2025; Pham et al., 2023; Picone et al., 2022; H. Wang et al., 2024; Y. Wang et al., 2023; Yu et al., 2023; H. Zhang et al., 2023; S. Zhang et al., 2024; Y. Zhang et al., 2023), due to its widespread agricultural use and associated health risks. Other targets, such as pathogens (K. S. Wang et al., 2024; Xu et al., 2020; Zhao et al., 2022), antibiotics (Han et al., 2024; Jiang et al., 2024; Liang et al., 2022; Nguyen et al., 2024; Sun et al., 2023; Zhang et al., 2020), and uric acid (Verma et al., 2022; Yang et al., 2024), have been explored to a lesser extent, and the field of toxin detection remains largely underdeveloped. SERS has emerged as a powerful analytical technique for the rapid and sensitive detection of bacterial toxins, offering significant advantages over conventional methods including real-time analysis, minimal sample preparation, and exceptional sensitivity. Recent advances in SERS-based biosensors have demonstrated remarkable detection capabilities across a wide range of bacterial toxins. For Shiga toxin detection, a novel nanopattern fabricated by electron beam lithography with remarkable plasmonic properties has achieved limits of detection (LOD) as low as 2 pM using a monoclonal antibody immobilized onto the SERS substrate via physical adsorption (Rippa et al., 2025). Staphylococcal enterotoxin B detection has been accomplished with LODs of 0.001 ng/mL using lateral flow immunoassays in buffer solutions (Hwang et al., 2016), and staphylococcal enterotoxin C has been detected at 0.55 pg/mL using Au-Ag Janus@Au nanoparticles(Xu et al., 2023). Botulinum toxin detection has been achieved through multiple SERS approaches, with aptamer-based sensors reaching 2.4 ng/mL LOD and (Subekin et al., 2023) immunoassay formats achieving 0.7–1.2 ng/mL in phosphate-buffered saline and human serum(Lim et al., 2019). For cholera toxin, affinity peptide-based SERS sensors have demonstrated high sensitivity of 3.51 pg/mL (Lim et al., 2018). Pyocyanin, a toxin

biomarker from Pseudomonas aeruginosa, has been detected using gold nanostar-based solution SERS with LODs of 0.05 nM in drinking water and 0.4 nM in biological fluids (Atta and Vo-Dinh, 2023). These performance metrics demonstrate that SERS technology provides a versatile platform for bacterial toxin detection across diverse sample matrices. The integration of various nanostructured substrates, from gold nanostars to photonic crystals, along with specific recognition elements such as antibodies and aptamers, has enabled the development of highly sensitive and selective SERS biosensors capable of meeting the stringent requirements for food safety and clinical diagnostics applications (Usman et al., 2023). Within the niche of flexible SERS for toxin sensing, to the best of our knowledge there is only one prior report: an aptamer-assisted Ag-nanoparticle–loaded bacterial cellulose membrane (BCM) sensor for dinophysistoxin-1 (DTX-1). That study achieved a limit of detection (LOD) of 9.5×10^{-10} M and showed 95.8–108.2 % recoveries in oyster and mussel extracts (You et al., 2023). Beyond this single example—targeting a small, algal toxin—we found no reports of flexible SERS applied to bacterial protein toxins (You et al., 2023). *Shiga toxin producing Escherichia coli* (STEC) is a major foodborne pathogen responsible for severe gastrointestinal infections and life-threatening complications such as hemolytic uremic syndrome (HUS) (Centers for Disease Control and Prevention, 2024; World Health Organization, 2023; Freedman et al., 2023). STEC strains produce Shiga toxins (Stxs), structurally and functionally like those produced by *Shigella dysenteriae* (Menge, 2020). Stxs are highly potent, with toxic effects observed at extremely low concentrations. In cell cultures, cytotoxicity can occur at levels as low as picomolar (pM) (Arfilli et al., 2015; Brigotti et al., 2019; Varrone et al., 2021) as in the case of Raji or Vero cells that have been used to detect the presence of Stx2 in serum or in feces. In animal models, even 15–50 ng per kilogram intravenous doses can be lethal or cause severe symptoms as in mice or baboons (Stearns-Kurosawa et al., 2010; Watanabe-Takahashi et al., 2018). In humans, although an exact toxic blood concentration is not clearly defined, very small amounts—in the low nanogram range— circulate in blood and are sufficient to trigger serious conditions such as HUS (Varrone et al., 2021). In STEC-infected patients, Stxs are associated to circulating cells at nanomolar concentrations (0,2-2 nM, neutrophils) whereas picomolar concentrations of Stxs (30–90 pM) are present in sera (Varrone et al., 2021). Interestingly, a small fraction of serum Stxs is vesicle-bound and causally related to the development of HUS (Maurizio, 2020; Varrone et al., 2021). These toxins belong to the AB5 family of protein toxins, consisting of a catalytically active A subunit (32 kDa) and B pentamer (8 kDa each). The B subunit binds to the cellular receptor globotriaosylceramide (Gb3Cer), facilitating the internalization of the A subunit, which then cleaves a specific adenine residue in the 28S rRNA of the 60S ribosomal subunit, irreversibly inhibits protein synthesis, and induces cell apoptosis (Menge, 2020; Centers for Disease Control and Prevention, 2024; World Health Organization, 2023). Two primary variants of Stxs, Stx1 and Stx2, share structural similarities but exhibit distinct pathogenic effects. Stx1 is often associated with less severe gastrointestinal symptoms, including diarrhea and abdominal cramps, and is less frequently linked to serious complications. In contrast, Stx2 is considerably more cytotoxic and strongly associated with HUS development, particularly in young children (Freedman et al., 2023). It causes significant endothelial damage, especially in the kidneys, triggering platelet activation, microthrombi formation, and ultimately acute renal failure. As Stx2-producing bacterial strains present a higher risk of severe disease, differentiating between Stx1 and Stx2 is essential for early diagnosis, risk assessment, and clinical decision-making. Ruminants, particularly cattle, are the primary reservoirs of STEC, although other mammals and birds can also act as carriers. Transmission to humans primarily occurs through consuming contaminated food and water, including undercooked meat, unpasteurized dairy products, fresh produce, and contaminated drinking water or water used for recreational activities (such as swimming pools, lakes, or rivers). Cross-contamination during food handling is another common cause of infection. Once ingested, STEC adheres to the intestinal mucosa, leading to diarrhea and the release of systemic toxins (Freedman et al., 2023; Melinte et al., 2024; Robert and Wiels, 2021). Given the low infectious dose of STEC and its ability to persist in environmental reservoirs such as water and soil, early and accurate detection of Stxs is essential for disease prevention and clinical management. Conventional diagnostic methods, including culture-based assays, enzyme immunoassays, and PCR, provide reliable identification but often require specialized equipment, trained personnel, and lengthy processing times (Brown et al., 2023; Hameed et al., 2018; Hamm et al., 2019; Koutsoumanis et al., 2020; Springer Browne et al., 2021; Yang et al., 2021, 2022; Zhu et al., 2022). The ability to distinguish structurally similar biomolecules, such as Stxs, presents a key challenge in molecular diagnostics, especially when subtle differences hold significant clinical implications. Recent advances in SERS biosensing technologies have paved the way for highly accurate and sensitive detection of Stx2. Moreover, to the best our our knowledge, it was our team that uniquely succeeded in realizing a sensor capable of achieving such performance (Rippa et al., 2025; 2022). In this study, we asses the performance of gold nanoparticle-coated Kapton as flexible SERS sensors, focusing on their ability to detect and differentiate highly similar molecular signatures. As a case study, we examine three subtypes of Stxs (Stx1, Stx2, and cleaved Stx2), by analyzing their spectral profiles to evaluate the sensor's detection capabilities. The ability to detect and differentiate these toxins with high specificity is clinically relevant, as varying strains necessitate distinct therapeutic strategies. For example, STEC-infected patients with blood Stx2 are at higher risk of developing HUS than patients with circulating Stx1 (Ardissino et al., n.d.) therefore early discrimination of the two toxins is important for patients' management. If we consider Stx2, the cleaved and native forms share the same cytotoxic activity for eukaryotic cells, but largely differ in pathogenicity due to their different abilities to interact with human circulating cells and the complement system during early toxemia, a crucial step in the pathogenesis of HUS in STEC-infected children (Brigotti et al., 2019). Native and cleaved Stx2 forms circulate simultaneously in the blood of STEC-infected patients (Varrone et al., 2023) triggering two different mechanisms: the release of pathogenic extracellular vesicles by blood cells (native Stx2) and the activation of the complement system (cleaved Stx2) (Brigotti et al., 2019). Their contributions to the pathogenesis of HUS is based on vesicle-mediated toxic effects (native Stx2) or on the complement-mediated lytic activity (cleaved Stx2) on renal target cells. The detection of the amounts and relative proportion of the different Stx2 forms in patients' blood would provide important information for clinical diagnosis and management. However, from an analytical standpoint, our emphasis is on demonstrating that the sensor is sensitive enough to identify even the most subtle spectral discrepancies. To validate this capability, we apply Principal Component Analysis (PCA), which successfully differentiates the three toxin variants based solely on their Raman spectra. This finding highlights not only the potential of our Kapton-based SERS sensor in pathogen detection but also its ability to resolve fine molecular variations. Furthermore, one of the most promising aspects of our study is the sensor's ability to achieve an extremely low LOD, enabling the identification of even trace concentrations of the analyzed toxins. This high sensitivity is essential for early diagnosis and the prevention of serious health complications. Since Stxs can be present in human blood during infection, the flexible sensor could be used as a patch with integrated microneedles for minimally invasive blood sampling (Jiang and Lillehoj, 2020). Such a system could enable fast, point-of-care diagnostics in clinical environments.

2. Materials and methods

2.1. Chemicals

Hydrogen tetrachloroaurate (III) trihydrate ($HAuCl_4 \cdot 3H_2O$), trisodium citrate ($Na_3C_6H_5O_7 \cdot 2H_2O$, 99 %), ethanol absolute anhydrous and

toluene were purchased from Carlo Erba Reagents. 4-Mercaptobenzoic acid (4MBA, 99 %) and phosphate-buffered saline (PBS, pH 7.4, liquid) were obtained from Sigma-Aldrich. Polyimide tape (Kapton) was supplied by MaoXinTek.

2.2. Synthesis of gold nanoparticles

Gold nanoparticles (Au NPs) stabilized with citrate were synthesized by reducing tetrachloroauric acid. First, 1 mL of 1 % sodium citrate was added to 97 mL of boiling $HAuCl_4$ solution (10^{-4} g/mL) while stirring. The mixture was boiled for 10 min (Grzelczak et al., 2008; Sharma et al., 2024). While still boiling, 1 mL of sodium citrate and 1 mL of $HAuCl_4$ solution were added every 2 min, repeated three times. The solution was then heated at 100 °C for another 20 min before cooling naturally. Finally, 24 mL of the nanoparticle solution was centrifuged at 8000 rpm for 10 min, and the precipitate was redispersed in a 50:50 deionized water-ethanol solution to form the Au NP layer (Lin et al., 2020).

2.3. SERS substrate fabrication and morphological characterization

The SERS substrate was fabricated by assembling Au NPs at the interface between two immiscible liquids using the Langmuir–Blodgett self-assembly technique (Lin et al., 2020). First, 8 mL of toluene was carefully layered over 80 mL of water to create a stable liquid-liquid interface. Then, 4 mL of water-ethanol-dispersed Au NPs were slowly injected using a mechanical syringe pump at 3 mL/h. As the toluene evaporated, the Au NPs self-assembled into a monolayer at the interface (SAM). Finally, this monolayer was transferred onto Kapton tape, to obtain a gold nanoparticles flexible tape (GNPsFT) (Zhou et al., 2023a). The nanostructures fabricated were characterized morphologically by making use of scanning electron microscopy (SEM, Raith 150) and via atomic force microscopy (AFM) in a semi-contactless configuration on a 5×5 μm^2 area.

2.4. SERS measurements

SERS spectra were recorded using a QE Pro-Raman system (Ocean Optics) with an Olympus BX51 upright microscope in a backscattering setup. The system operated at a 785 nm laser wavelength, with a 1200 lines/mm grating and a 25 μm input slit. A 50 × objective (N.A. = 0.75) and a laser power of 12 mW were used for measurements. To estimate the SERS enhancement factor (EF), approximately 40 spectra were collected from different points on both the GNPsFT coated with a 4-MBA SAM and a Kapton flexible tape (KFT) with bulk 4-MBA powder, in the 400–1800 cm^{-1} range with a 10-s acquisition time. The 4MBA SAM was prepared by applying 10 μL of 10 mM 4-MBA in ethanol at 4 °C in a humid environment for 12 h. The sample was then rinsed with water and ethanol to remove unbound molecules. To estimate the inter-batch reproducibility, we tested three independent batches; that is, three gold layers were prepared on different days using the same protocol and then transferred onto Kapton tape. For each batch, 10 μL of 10 mM 4-MBA in ethanol was deposited at 4 °C in a humid environment for 12 h, and at least 40 measurements were taken at different points on each sample. For Stxs detection, approximately 40 SERS spectra were collected per toxin in the 350–1400 cm^{-1} range with a 10-s acquisition time. All spectra were baseline-corrected and averaged using Omnic software.

2.5. SERS detection of toxins

2.5.1. Shiga toxins

Stx1 and Stx2 were produced by E. coli C600 (H19J or 933W, respectively) and purified by receptor analog affinity chromatography as described in literature (Matussek et al., 2003; Ryd et al., 1989). Both toxins were further purified on ActiCleanEtox columns (SterogeneBioseparations, Carlsbad, CA, USA) to remove contaminant bacterial endotoxin. Cleaved Stx2 (Brigotti et al., 2019) was obtained by incubating native Stx2 (120 μg) with trypsin (1 μg) in 100 μL-PBS (1 h at 37 °C) followed by the addition of phenylmethylsulfonyl fluoride (14 ng) as inhibitor (10 min at 37 °C, final reaction volume 120 μL). Purified toxins were stored at −80 °C in small aliquots and diluted with PBS before each assay.

2.5.2. Fingerprint analysis

To obtain characteristic SERS peaks for each toxin, solutions were prepared both in PBS and human serum at a concentration of 1047 ng/mL. The PBS solutions were used to obtain representative SERS peaks specific to each toxin, while the solutions in human serum allowed for the identification of toxin peaks that remain detectable within the complex serum matrix. A droplet of pure human serum was also deposited under identical conditions to serve as a control. Droplets of these solutions were deposited directly onto the substrates (a schematic representation in Fig. 1) and incubated overnight in a humid chamber at 4 °C. The samples were then washed with bi-distilled water and dried with N_2 gas before SERS measurements.

2.5.3. Limit of detection

To determine the LOD, the same procedure as in Section 2.5.2. was followed. Measurements were taken at toxin concentrations ranging from 2 to 1047 ng/mL. After incubation, the nanosensor was washed, and SERS spectra were recorded.

2.6. Data analysis

Spectral data were processed and analyzed using Origin2023 software. Preprocessing steps included baseline correction and spectral normalization to enable reliable comparisons among samples. Characteristic toxin peaks were identified and assigned within Origin2023 to ensure consistent interpretation across replicates. To distinguish between Stx1, Stx2, and cleaved Stx2, PCA was employed as a dimensionality reduction method that retains the most relevant variance within the dataset. PCA was carried out in R (version 2024.04.2 + 764) using the ChemoSpec package. Subsequently, k-means clustering was performed on the first two principal components (PC1 and PC2) using the cluster package in R. This method was selected as an initial unsupervised approach to evaluate whether spectral variations were sufficient to separate the toxin types into coherent clusters (Ikotun et al., 2023; Islam et al., 2021). Each resulting cluster was subsequently

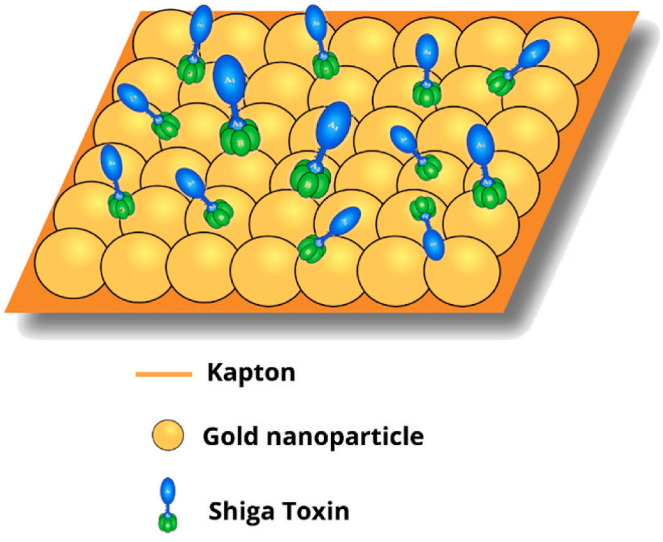

Fig. 1. Schematic representation of the Stx2 deposition on the GNPsFT surface via physical adsorption.

labeled according to the corresponding toxin subtype, and the output was assessed for consistency and discriminative power. While other clustering methods were also explored during the analysis, k-means was ultimately chosen for its clarity, efficiency, and compatibility with PCA-driven separation tasks. Finally, one-way analysis of variance (ANOVA) was applied to PC1 and PC2 via the stats package in R to statistically evaluate whether the observed spectral differences between toxin groups were significant. Each principal component was tested separately to determine the contribution of toxin type to the overall spectral variation.

3. Results and discussion

3.1. SERS substrate characterization

Au NPs were synthesized using the sodium citrate reduction method, ensuring a uniform size distribution. A large-scale SAM of Au NPs was then formed at the interface of two immiscible liquids using the Marangoni effect (Lin et al., 2020) as shown in Fig. 2 (a) and transferred on the Kapton tape (Fig. 2 (b)). The SEM (image in Fig. 2 (c)) confirms that the Au NPs have a uniform size distribution, with an average diameter of 37 ± 4 nm (measured by software ImageJ) and Relative Standard Deviation (RSD%) value is 11.2 %. Moreover, based on SEM analysis, the Au NP layer is evenly distributed, with no noticeable clustering, this is essential for enhancing local electromagnetic fields, which in turn strengthens the Raman signal and improves detection sensitivity. Atomic force microscopy (AFM) revealed that the Au nanoparticle film forms a continuous and uniform layer with strong adhesion to the Kapton substrate (Giménez et al., 2002; Philip and Mohan, 2024) (Fig. 2 (d)). The three-dimensional profiles confirm well-defined nanostructures and a high density of plasmonic hotspots (Jiang et al., 2004; Kimura et al., 2013; METAL NANOPARTICLES ON POLYMER SURFACES: *1. 747*, 2001; Xu et al., 2007) (Fig. 2 (e)). Notably, a unidirectional arrangement of nanoparticles was observed, suggesting effects related to the propagation of the adhesive layer during deposition, as reported in other nanostructured films(Ahmed et al., 2017; Caillard et al., 2013; Georgiev et al., 2013; Hosny et al., 2014). These morphological features, including optimal nanoparticle size and surface homogeneity, are critical for efficient SERS performance and analyte adherence.

3.2. Gold nanoparticles flexible tape enhancement factor

The SERS capabilities of the self-assembled gold nanoparticle film on our flexible substrate were analyzed using the 4MBA molecule as a Raman probe. As shown in Fig. 3 (a), the SERS spectrum of 4MBA displays distinct fingerprint characteristics. A strong peak at 1079 cm^{-1} corresponds to in-plane ring breathing and C-S stretching vibrations, while another peak at 1588 cm^{-1} is linked to the C-C stretching vibration of the aromatic ring (Rippa et al., 2017, 2024; Zhou et al., 2023a). By comparing the SERS spectrum with the bulk Raman spectrum of 4MBA (Fig. 3), we calculated the Enhancement Factor (EF) for the SERS substrate using equation E.F. = $[(I_{SERS}/I_{RAMAN})$ x $(N_{RAMAN}/N_{SERS})]$ where $I_{SERS(1079)} = 27678$ and $I_{RAMAN(1079)} = 277$ while $N_{RAMAN} = 2.7 \times 10^{11}$ and $N_{SERS} = 3.9 \times 10^{6}$ are based on our previous studies (Rippa et al., 2022; Zhou et al., 2023; 2022). The EF value was determined to be 6.9×10^{6}, confirming the high sensitivity of the SERS substrate. To assess uniformity, we collected SERS spectra from random points on the substrate. The Raman spectra from these points were highly consistent, with no noticeable shifts or variations in the characteristic peak. Generally, the reproducibility of the SERS substrate was evaluated by calculating the RSD%. In this case, the RSD% values for the peaks at 1079 cm^{-1} and 1588 cm^{-1} were 7.4 % and 8.2 %, respectively. To estimate inter-batch reproducibility, three independent batches were tested, resulting in the three spectra shown in Fig. 3(b) and the quantitative data reported in Table 1. The inter-batch RSD% for the enhancement factor calculated across the batches was 6.5 %, and the overall mean E.F. across batches was $7x10^{6}$, demonstrating good reproducibility between independent sensor preparations. In our previous work (Zhou et al., 2023) we evaluated the stability of an analogous Au NP self-assembled SERS substrate on silicon, observing only ~10 % signal loss for 4MBA after three months under ambient conditions. Since the fabrication protocol and enhancement factor are comparable, we expect similar long-term stability. Literature further supports this, showing Au-based SERS substrates typically retain performance for months to over a year when stored in dry, room-temperature conditions, with <15 % signal decrease (Shao et al., 2024; Sweedan et al., 2024; Wiriyakun et al., 2016; Xing et al., 2022). Kapton's chemical and thermal stability further reinforces its suitability for field applications (McDonnell et al., 2023).

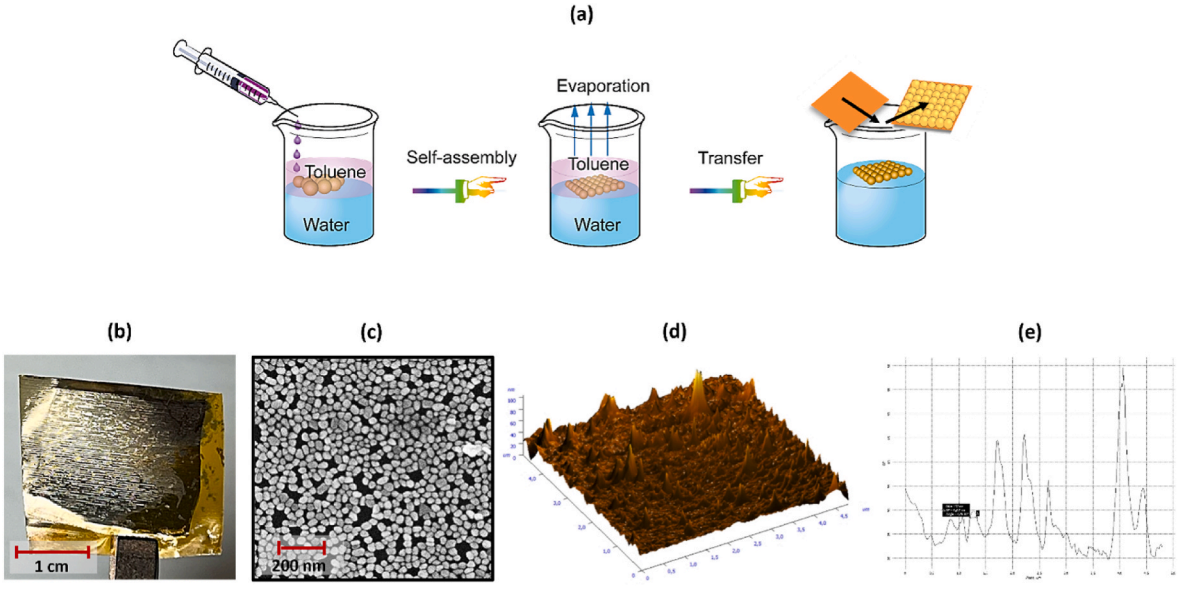

Fig. 2. Gold nanoparticles self - assembled monolayer on the flexible substrate: (a) Preparation of flexible SERS sensor. (b) Final photograph of the GNPsFT. (c) SEM image of the fabricated Au NPs layer on the Kapton. (d) 3D AFM scan from 5 × 5 μm^2 area. (e) Cross sectional profile analysis. (For interpretation of the references to color in this figure legend, the reader is referred to the Web version of this article.)

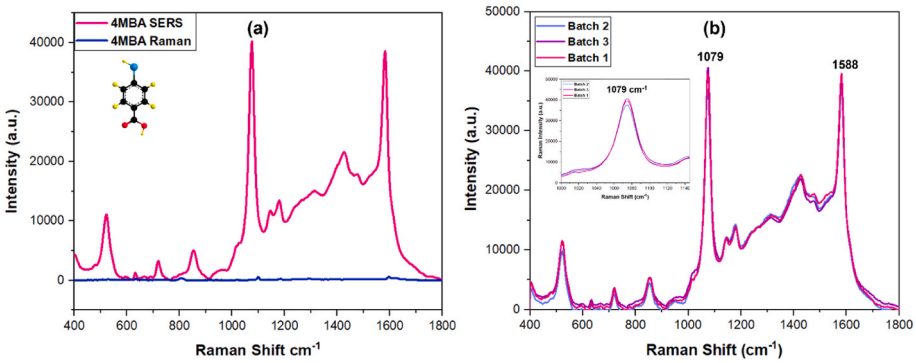

Fig. 3. (a) EF evaluation: Raman (blue) and SERS (magenta) spectra of 4MBA powder on the kapton tape and 4MBA solution (10 mM) on the gold nanoparticles layer attached to kapton tape, respectively. (b) Inter-batch variability: Representative SERS spectra of 4MBA solution (10 mM) obtained from three independent gold nanoparticle layers transferred onto Kapton tape, prepared on different days under identical conditions. (For interpretation of the references to color in this figure legend, the reader is referred to the Web version of this article.)

Table 1
Summary of SERS substrate reproducibility across three independent fabrication batches. For each batch, the enhancement factor (E.F.), mean intensity of the characteristic 4MBA peak at 1079 cm^{-1}, and intra-batch relative standard deviation (RSD%) calculated from 40 measurements are reported.

Batch	E.F.	I_{MEAN_1079}	Intra_batch_RSD %
1	6.9 x 10^6	27678	7.4 %
2	6.4 x 10^6	25637	6.8 %
3	7.3 x 10^6	29231	9.1 %

3.3. *Stx2 fingerprint*

Detecting Stx2 accurately is essential for diagnosing and managing infections caused by STEC. The SERS analysis of Stx2 revealed a unique spectral pattern (Fig. 4 (a)), highlighting the toxin's specific structural and chemical features in PBS. A tentative assignment of the toxin SERS bands is provided in Table 2. The SERS fingerprint spectrum of Stx2 provides detailed insights into its molecular structure and vibrational modes. The observed bands are consistent with the expected chemical and structural features of a complex protein composed of multiple subunits. Bands in the region 500–540 are linked to disulfide bonds and that at 547 cm^{-1} to tryptophan. This shows that S–S bonds formed by cysteines residues keep the tertiary shape of Stx2 stable. Peaks observed in the region between 600 and 750 cm^{-1} have been attributed to tyrosine (at 657 cm^{-1}) in the region of the Fermi's resonance and to the C-S stretching of methionine (724 cm^{-1}). The prominent peak at 1265 cm^{-1}, attributed to the amide III α-helix modes, confirms the presence of well-ordered secondary structures, indicating a substantial contribution of α-helices to the toxin's overall architecture. In addition, the strong band at 1141 cm^{-1}, assigned to C–N stretching and CH bending, emphasizes the contribution of the polypeptide backbone to the overall Raman signature. The assignment of bands at 1345, 1375, and 1419 cm^{-1} to CH_2/CH_3 bending and COO^- vibrations suggests significant involvement of amino acid side chains. Altogether, the vibrational fingerprint obtained by SERS provides a comprehensive molecular signature of Stx2, capturing both its backbone architecture and the specific contributions from side-chain functionalities. The SERS fingerprint spectrum was obtained also in the presence of a biological fluid such as human serum (Fig. 4 (b)) showing the same peaks observed in the presence of PBS, even though changes in intensity or shape of some bands were recorded (Table 2). In particular, the band related to the amide III α-helix modes (1265 cm^{-1}) appeared less structured and blunted, as well as the subsequent region comprising the peaks at 1345, 1375 and 1419 cm^{-1}. Interestingly, the band attributed to the C-S stretching of methionine (724 cm^{-1}) is more prominent and sharper under this condition. In conclusion, protein fouling due to the addition of human serum while giving measurable changes did not significantly alter the spectral pattern of the toxin.

3.4. *Limit of detection of gold nanoparticles flexible tape*

To evaluate the developed sensing system's performance in detecting Stx2, we determined its LOD in the presence and in the absence of human serum. For the concentration used (2, 3, 5, 50, 1047 ng/mL in PBS; and 50, 100, 500, 1047 ng/ml in serum), we collected approximately 40 measurements and used the average Raman intensity to get statitically reliable results. We evaluated the experiment's robustness by

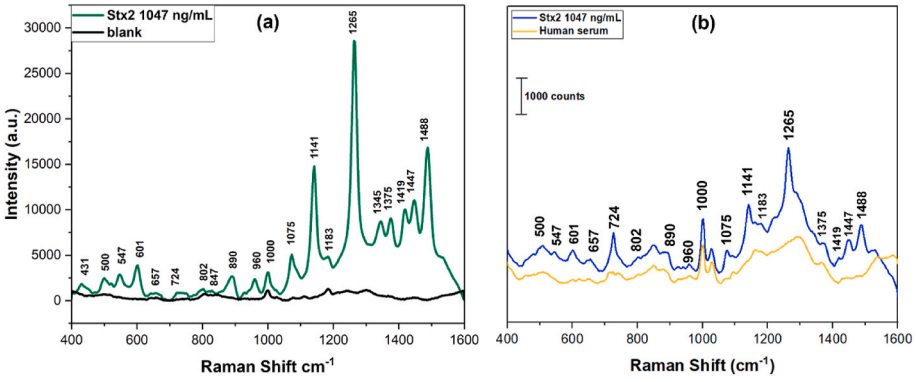

Fig. 4. (a) SERS fingerprint of Stx2 in PBS: spectrum of Stx2 in PBS on the Au NP flexible tape (green) compared to the blank spectrum of the Au NP layer on Kapton tape (black). (b) SERS fingerprint of Stx2 in human serum: spectrum of Stx2 in human serum on the Au NP flexible tape (blue) compared to the spectrum of human serum alone (yellow). (For interpretation of the references to color in this figure legend, the reader is referred to the Web version of this article.)

Table 2
Tentative assignment of the main peaks observed in the SERS spectrum of Stx2, recorded both in PBS and human serum. The table lists characteristic vibrational modes and their corresponding wavenumbers, providing a detailed interpretation of the spectral features and highlighting any intensity or shape changes observed in biological fluid.

Wavenumber (cm^{-1})	Assignment Stx2 on flex substrate	Peak changes in the presence of human serum	References
500	Protein S-S	–	(Benson K et al., 1967; Chen C. M and Lord R. C, 1976; Lin and Koenig, 1976; Nakamura et al., 1997)
547	Protein S-S Trp	Fare clic o toccare qui per immettere il testo. blunted Fare clic o toccare qui per immettere il testo.	(Lin and Koenig, 1976; Nakamura et al., 1997; Chen C. M and Lord R. C, 1976) (Fazio B et al., 2016; Rippa et al., 2022; Szekeres and Kneipp, 2019)
601	Ring breathing	blunted	Zhu et al. (2011)
657	Tyr ring deformation	–	(Lin and Koenig, 1976)
724	Tyr Ile ν(C–S)T Met C–S stretching	enhancedFare clic o toccare qui per immettere il testo.	Fazio et al. (2016) (Huang et al., 2020; Jess et al., 2007; Kudelski, 2005)
847	Tyr	enhanced	(Chen C. M and Lord R. C, 1976; Fazio et al., 2016; Lin and Koenig, 1976)
890	CS bond or aromatic ring Trp	–	(He et al., 2023; Szekeres and Kneipp, 2019
960	Phosphate (P–H bending and P–O stretching)	blunted	Aitekenov et al. (2022)
1075	Strong C9 H's stretch causing a strong inner ring distortion on C9, C10, C11, wagging of H39, asymmetric stretch of benzene ring at C11, wagging of H40 n(Ca-N) Trp	–	(Chou et al., 2008; He et al., 2023; Fazio et al., 2016)
1141	ν(CN) Stretching (CN) protein Tyr In-plane CH bending, ring CH bending	blunted Fare clic o toccare qui per immettere il testo.	Chou et al. (2008) (Biswas et al., 2023) Fazio B et al. (2016) (Huang et al., 2020)
1265	Amide III alpha helix	less structurated and blunted	(Brigotti et al., 2019; Fraser et al., 2004; Loxd and Yu, 1970)
1345	Wagging (CH2, CH3)	–	Willets (2009)
1375	δ (COO), vs (COO–)	–	Shahid et al. (2024)
1419	Bending of CH_2/ CH_3 groups and/or C–N stretching	Fare clic o toccare qui per immettere il testo. blunted	(Botti et al., 2018; Madzharova et al., 2016; Simeral et al., 2021)
1447	Stretching C-H	–	(Biswas et al., 2023)
1488	Tryptophan ring modes or C=C/ C=N stretches in proteins	Fare clic o toccare qui per immettere il testo. blunted	Barhoumi and Halas (2010) Negri and Schultz (2014)

Table 2 (*continued*)

Wavenumber (cm^{-1})	Assignment Stx2 on flex substrate	Peak changes in the presence of human serum	References
		Fare clic o toccare qui per immettere il testo.	

performing independent runs, each utilizing a sensor sourced from distinct manufacturing batches. The findings remained consistent across these independent trials, supporting the reliability of the observed outcomes. The sensor's performance in detecting Stx2 was evaluated by analyzing the Raman intensity at 1265 cm^{-1}, Amide III vibration corresponding to α-helices (Brigotti et al., 2019; Fraser et al., 2004; Loxd and Yu, 1970). As shown in Fig. 5 (a) and in Fig. 5 (c), the SERS signal intensity increases with higher toxin concentrations, demonstrating a clear dose-dependent response. The relationship observed between the SERS intensity and the toxin concentration further validates the quantitative capabilities of the developed system.

In Fig. 5 (b) and 5 (d), the y-axis shows the net SERS intensity of the toxin's highest peak at 1265 cm^{-1}. The experimental data exhibit a good linear relationship between the intensity and the logarithmic values of the toxin concentration in the range 3–1047 ng/mL (PBS) or 50–1047 ng/ml (serum). The best-fit equations, $I_{Stx2} = a\,\mathrm{Log}[Stx2]+b$, were obtained with $a = 21566$, $b = -11146$ or $a = 758.66$, $b = -1146$, and R^2 values of 0.9604 or 0.97 (green line in Fig. 5 (b) and blue line in Fig. 5 (d)) with PBS or serum, respectively. The LOD was calculated by using the equation $[(3 \times \sigma)/a]$ (Mocák et al., 2009; Shrivastava and Gupta, 2011) where σ is 166 and represents the standard deviation of the blank control (Rippa et al., 2024; Suleimenova et al., 2024; Tuckmantel Bido and Brolo, 2023). Using this approach, the LOD for Stx2 was determined to be 15 pM in the presence of PBS or 67 pM in the presence of human serum. To the best of our knowledge, we are the first to detect Stx2 with an ultra-low LOD using a flexible SERS substrate made via a simple, cost-effective bottom-up method (Lin et al., 2021; Zhou et al., 2021). Importantly, the value obtained in PBS is similar or below the lower limits of clinically relevant Stx concentrations measured in stools and sera of STEC-infected patients. Indeed, bead-ELISA measurements reported toxin levels in stools ranging from 0.71 to 10.44 ng/mL (approximately 10–150 pM) for Stx1 and 2.75–51.61 ng/mL for Stx2 (approximately 40–750 pM) (Armstrong et al., 2018a). The higher LOD obtained in the presence of human serum fits within the range of concentrations of Stx found in patients' sera and detected by ELISA: 10–200 pM (Stx1) and 30–90 pM (Stx2) (Brigotti et al., 2020 Thromb Haemost, 2020; 120:107–120). Finally, Stx have been observed bound to polymorphonuclear leukocytes at very high concentrations (nanomolar range) (Varrone et al., 2021; Brigotti et al., 2011). These findings indicate that our system provides a sensitivity suitable for the determination of clinically relevant Stx concentrations, thus supporting its potential for application in real diagnostic settings in the earlier stages of the disease. As shown in Table 3, our flexible SERS substrate is comparable to or outperforms many other flexible platforms reported in the literature, both in terms of detection performance and fabrication simplicity. We also checked how reproducible the results were by calculating the RSD% at each concentration. This helped us measure the space homogeneity of the sensor. The RSD% values were 7.23 % at 2 ng/mL, 6.67 % at 3 ng/mL, 8.54 % at 5 ng/mL, 12.5 % at 50 ng/mL, and 11.9 % at 1047 ng/mL, showing good repeatability even at low toxin levels. The low variation across concentrations indicates strong reliability within the sample. Table 4 demonstrates that our method works better than both traditional techniques (e.g., PCR, Lateral Flow Immunoassay, and ELISA) and newer strategies (such as LSPR and SPRi), emphasizing its enhanced sensitivity.

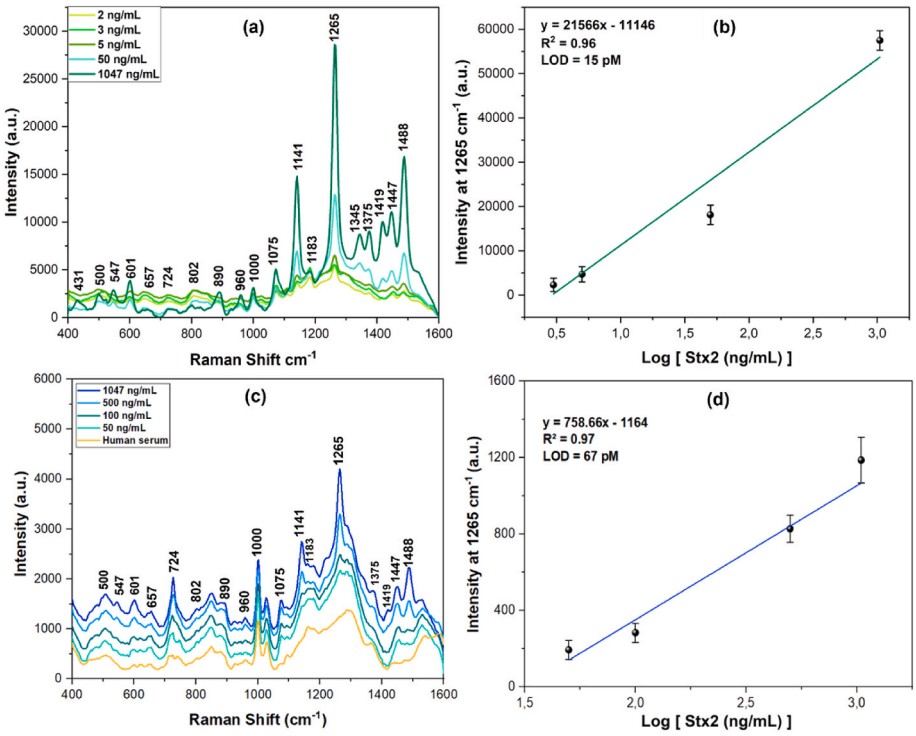

Fig. 5. SERS measurements of the Stx2: (a) Comparison between the spectra of the Stx2 at increasing concentrations of Stx2 in PBS. (b) Calibration curve achieved by plotting the 1265 cm^{-1} peak intensity vs the logarithmic of toxin concentrations and linear fit associated with data (green line). (c) Comparison between the spectra of the Stx2 at increasing concentrations of Stx2 in human serum. (d) Calibration curve achieved by plotting the 1265 cm^{-1} peak intensity vs the logarithmic of toxin concentrations and linear fit associated with data (blue line). (For interpretation of the references to color in this figure legend, the reader is referred to the Web version of this article.)

Table 3
A list of flexible SERS substrates fabrication methods and SERS performance.

Substrate	Composition	Fabrication method	Analytes	E. F.	Uniformity (RSD)	LOD	Ref.
Kapton tape	Au NPs	Self-assembly	4MBA and Shiga toxins	10^6	≤12.5 % for 40 random points	15 pM in PBS and 67 pM in human serum	*This work*
PDMS	Core-shell Au@Ag nanoparticles	Self-assembly	Bacteria	10^7	–	2.79 CFU/m E. coli, 3.42 CFU/m S. aureus and 4.52 CFU/mL P. aeruginosa	Zhou et al. (2025)
PDMS	Ag NRs	Glancing angle deposition	Thiram	10^8	Within 20 %	2.4×10^{-9} g cm^{-2}	Kumar et al. (2017)
PDMS	Au NPs on colloidal particle arrays	Nanosphere lithography, soft lithography	BT	10^3	–	1 nM	Kang et al. (2013)
PDMS	Graphene/Au NPs	Graphene transfer/physical deposition	R6G	10^7	–	1 nM	Chen et al. (2017)
PDMS	Au nanostars	Dip-coating/detached	Benzenethiol	10^8	–	10 nM	Park et al. (2017)
PDMS	Ag NPs	AAO template and seeding deposition	4-MBA/TMTD	10^7	5.8 % for 30 random sites	1.6×10^{-9} g cm^{-2}	Wang et al. (2017)
Cellulose paper	AuNRs and NFC mixture	Gravity-assisted filtration method	R6G	–	≈4 % (from 221 pixels)	1 nM	Tian et al. (2016)
Cellulose filter paper	AgNPs	In situ synthesis by SILAR	RdB	10^9	4.2 % for 10 different substrates	10 pM	Kim et al. (2015)
Cellulose filter paper	Au NRs	Dropped on paper substrate	BPE	10^6	15 % (along the length of a fiber)	0.5 nM	Lee et al. (2011)
Cellulose paper	AgNPs	In situ synthesis by SILAR	RdB and 2-NT	10^7	≤11 % from 400 spots	1 pM	Chen et al. (2019)
PCL film	Ag film	Uniaxially stretching	4-MBT and MG	–	6.48 % for 45 random points	100 nM	Xu et al. (2017)
PMMA	Graphene/Ag-nanoflowers	Chemical reduction method	R6G	–	Lower than 10 %	0.01 pM	Qiu et al. (2017)
PVP	Ag NPs	One-step electronic reduction	4-ATP	10^9	–	0.1 pM	Wang et al. (2016)
Polyimide	Ag@Au NPs	In situ synthesis by chemical reduction and galvanic replacement	BPE and Thiram	10^7	8.7 % for 30 random points	1 nM	(Liu et al., 2020)

Table 4
Comparison with current technologies for Stxs detection.

Technique	Feature	Analytes	LOD	Ref.
SERS	Gold NPs self-assembled on kapton tape	Stx2	15 pM in PBS and 67 pM in human serum	*This work*
ELISA	Synthetic sample with antibody as receptor	StxB	90 ng/mL	Mirhosseini et al. (2022)
AlphaLISA	Bead-based immunoassay	Stx	0.5 ng/mL	(Armstrong et al., 2018ab)
Lateral Flow Immunoassay	Based on AuNP and CdTe QD	Stx2	25 ng/ml	Lu et al. (2020)
(mPCR) assay	Vero cells in a three-dimensional (3D) platform	Stx1, Stx2	32 ng/ml	To and Bhunia (2019)
LSPR	Gold nanoparticles bound to antibodies	Stx2	10 ng/mL	Yaghoubi et al. (2023)
LSPR	Cell surface oligosaccharides on glycol chips	Stx	10 ng/mL	Nagatsuka et al. (2013)
SPRi	Biochip with 50-nm gold film	Stx1, Stx2	50 ng/mL	(Karbalaee et al., 2025; Wang et al., 2020)
SPR	11-mercaptoundecanoic acid-modified Chip with protein G	Stx	9.8 ng/mL	Karbalaee et al. (2025)

3.5. PCA-based differentiation of three Stxs on the gold nanoparticles flexible tape

Traditional methods such as PCR and ELISA can struggle to differentiate between toxin variants and isoforms because they may share portions of their amino acid sequence as in the case of the Stx1/Stx2 comparison or the whole sequence as in the case of cleaved/uncleaved Stx2, leading to diagnostic challenges. Because Stx2 is the primary toxin responsible for severe disease, it is critical to have detection techniques that can precisely identify it. The fabricated plasmonic substrate was utilized to identify the SERS spectral fingerprints of three types of Stxs. Each toxin was applied to three separate areas of the same substrate at a concentration of 1047 ng/mL in PBS. Fig. 6 (a) displays the average SERS spectra obtained for Stx1 (orange line), Stx2 (light blue line), and cleaved Stx2 (green line) in PBS. PCA was applied to evaluate the spectral differences among Stx1, Stx2, and cleaved Stx2 in both PBS and human serum (Fig. 6 b and d). In PBS, the first two components accounted for 47 % (PC1) and 38 % (PC2) of the total variance, yielding three well-separated clusters corresponding to the different toxin subtypes. Similarly, in serum, the PCA model explained 58 % (PC1) and 16 % (PC2) of the variance, and again produced a clear separation of the three groups, despite the additional complexity of the biological matrix. The consistent clustering across both environments highlights the robustness of the flexible SERS platform and its ability to retain strong discriminative performance when moving from buffer to serum. The absence of overlap between groups confirms that the spectral differences captured by the PCA are sufficient for reliable toxin classification. Further validation through k-means clustering and ANOVA, reported in the Supplementary material, corroborates these findings and quantitatively supports the statistical significance of the group separation.

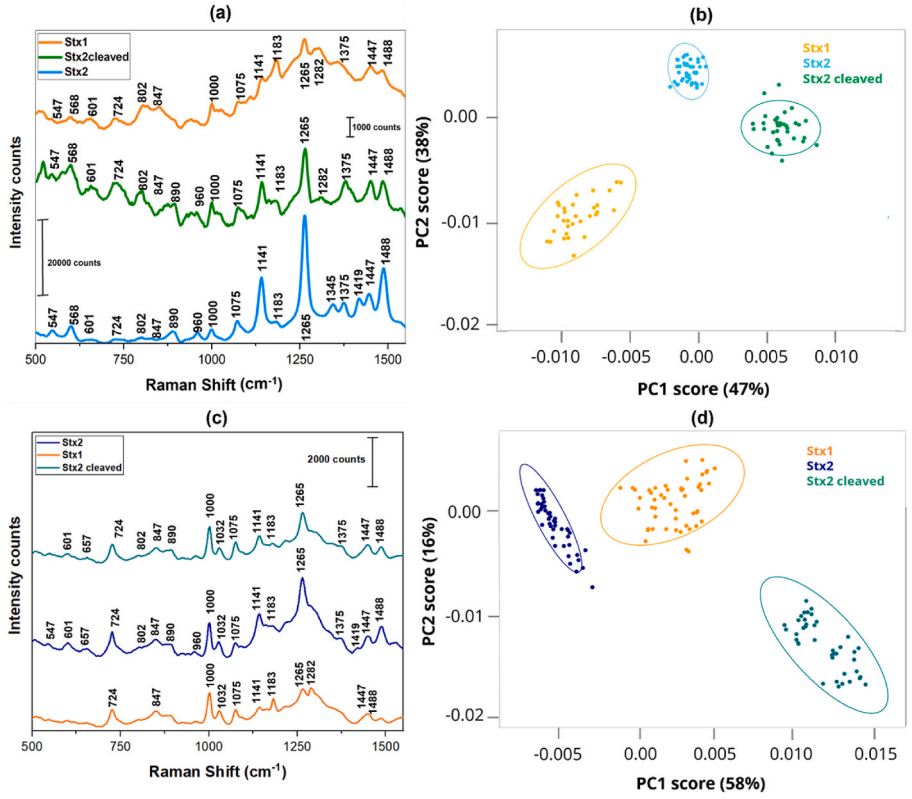

Fig. 6. Differentiation of three Stxs: (a) SERS spectra showing the characteristic signals of the three toxins in PBS (Stx1 as orange curve, Stx2 as light blue curve, cleaved Stx2 as green curve). (b) PCA of the SERS spectra for the three toxins in PBS (Stx1 as yellow dots, Stx2 as light blue dots, cleaved Stx2 as green dots). (c) SERS spectra showing the characteristic signals of the three toxins in human serum (Stx1 as dark orange curve, Stx2 as dark blue curve, cleaved Stx2 as dark green curve). (d) PCA of the SERS spectra for the three toxins in human serum (Stx1 as dark orange dots, Stx2 as dark blue dots, cleaved Stx2 as dark green dots). (For interpretation of the references to color in this figure legend, the reader is referred to the Web version of this article.)

Together, these results demonstrate that the sensor not only achieves accurate discrimination in a controlled buffer system but also maintains its high performance in complex biological samples, underscoring its potential for practical diagnostic applications.

Analysis of the SERS spectra revealed distinct fingerprint patterns for each toxin, highlighting differences in their molecular structures and chemical compositions. A detailed assignment of spectral peaks for Stx2 is provided in the previous paragraph (Table 2). The SERS spectra of Stx1, Stx2, and cleaved Stx2 show differences that reflect their structural variations. Stx2 (blue spectrum) shows sharp and intense peaks, especially at 1075, 1141, 1265, and 1488 cm^{-1}. These signals suggest that the Stx2 on the SERS surface might be differently arranged, with strong amide vibrations and contributions from side-chain groups like C–N and CH_2/CH_3 bending. Cleaved Stx2 (green spectrum) shows broader and weaker peaks, indicating local rearrangements after single proteolytic cleavage. Some features of Stx2 are still present but less defined in Stx1 spectrum (orange spectrum) that shows a weak signal and broad, poorly defined peaks, especially in the 1260–1300 cm^{-1} region, where α-helix bands are expected. In this region a new emerging peak at 1282 cm^{-1} is visible in cleaved Stx2 and well represented in Stx1. This may suggest a different arrangement of the toxin on the SERS surface or a different orientation compared to Stx2. Moreover, the peak related to methionine C-S stretching at 724 cm^{-1} is highly or moderately enhanced in cleaved Stx2 and Stx1 spectra, respectively. Additionally, the peaks at 890 and 960 cm^{-1}—associated with C–S bonds, Trp and Phosphate (P–H bending and P–O stretching) —are strong in Stx2, broad in cleaved Stx2, and absent or faint, respectively, in Stx1, likely because these groups are more internally located and harder to access. The peak at 1419 cm^{-1} is found only in Stx2. It may be due to CH_2/CH_3 bending and C–N stretching from exposed amino acid side chains. Finally, the peak at 1375 cm^{-1} is more intense and broad in cleaved Stx2 and Stx1 than in Stx2. However, the presence of many shared peaks suggests that core structural elements are conserved across the three toxins. Despite some shared spectral features, the SERS profiles of Stx1, Stx2, and cleaved Stx2 show distinct differences in peak intensity, shape, and presence—such as the 1419 cm^{-1} band exclusive to Stx2 or the 890 and 960 cm^{-1} peaks absent in Stx1. The described exclusive differences among toxins are conserved even in the presence of human serum (Fig. 6 (c)) although its addition modifies intensity and shape of other bands belonging to Stx1 and cleaved Stx2, as previously detailed for Stx2. In the presence of serum, peaks at 724 cm^{-1} are enhanced in Stx1 and cleaved Stx2 fingerprints, as described above for Stx2, whereas a common feature of the three toxins is the increased intensity of the band at 1000 cm^{-1}. With human serum, the peak at 1282 cm^{-1} is more defined in Stx1, whereas in cleaved Stx2 it concurs to the broadening effect already observed for the 1265 cm^{-1} band in Stx2. The differences between the three toxins observed under different conditions (with or without human serum) reflect underlying structural variations and confirm that each toxin has a unique vibrational fingerprint. This could be due to intrinsic differences in amino acid composition and protein conformation (Stx1 vs Stx2) or could be related to changes in the flexibility of the molecule after cleavage (Stx2 vs cleaved Stx2). Moreover, the different orientation of toxin molecules in binding the biosensor is a further element to be considered as source of signal diversity within the same toxin group or between the different groups. However, due to natural spectral variability and overlapping regions, visually distinguishing between the toxins in unknown samples remains challenging. To address this problem, PCA was applied to enhance the separation of spectral profiles. As shown in Fig. 6 (b), it reduced the complexity of the dataset by projecting it into a two-dimensional space defined by the first two principal components (PC1 and PC2). The resulting plot clearly displays three distinct clusters corresponding to Stx1 (yellow), Stx2 (light blue), and cleaved Stx2 (green), demonstrating successful differentiation among the subtypes. PC1 accounts for 47 % of the total variance, while PC2 explains 38 %, together capturing over 80 % of the dataset's variability—a level generally considered sufficient for robust classification. These results confirm that the combination of flexible SERS substrates with PCA enables accurate and label-free identification of Shiga toxin variants in PBS, without the need for antibody-based detection. To support the clustering performance observed in the PCA, we additionally performed k-means clustering and one-way ANOVA on the PCA-transformed data, confirming the statistical robustness of the toxin discrimination. Full results are provided in the Supplementary material.

4. Conclusions

This work reports a flexible, cost-effective SERS sensor based on Kapton® coated with self-assembled gold nanoparticles, achieving for the first time to the best of our knowledge, ultrasensitive, label-free detection and robust differentiation of Shiga toxins (Stx1, Stx2, and cleaved Stx2). The platform delivers an high detection limit (15 pM for Stx2), high inter-batch reproducibility (RSD% = 6.5 %), and effective spectral discrimination between closely related toxins using PCA.

To assess real-world applicability, the study was extended to human serum. Despite minor spectral variations, the fingerprint of Stx2 remained clearly detectable, with a calculated LOD of 67 pM—only slightly higher than in PBS and well within clinically relevant toxin levels. Importantly, the flexible, bottom-up SERS substrates enabled ultra-sensitive detection and reliable discrimination of Stx1, Stx2, and cleaved Stx2 in serum, with PCA, clustering, and ANOVA confirming distinct vibrational fingerprints.

Together, these findings demonstrate the robustness, sensitivity, and specificity of the approach, establishing flexible SERS technology as a powerful and practical tool for the early detection and discrimination of hazardous biomolecules in clinically and environmentally relevant scenarios.

CRediT authorship contribution statement

A. D'Avino: Writing – review & editing, Writing – original draft, Validation, Methodology, Investigation, Formal analysis, Data curation, Conceptualization. **A. Milano:** Writing – original draft, Methodology, Formal analysis. **V. Marchesano:** Writing – review & editing, Data curation. **B. Guilcapi:** Formal analysis, Data curation. **D. Sagnelli:** Writing – review & editing, Data curation. **M. Rippa:** Writing – review & editing, Data curation. **L. Zhou:** Investigation. **G. Rossi:** Data curation. **L. Consagra:** Analytical measurements. **M. Brigotti:** Writing – review & editing, Resources. **S. Morabito:** Writing – review & editing, Resources. **L. Petti:** Writing – review & editing, Supervision, Project administration, Conceptualization.

Informed consent

Informed consent was obtained from all individuals included in this study.

Ethical approval

The conducted research is not related to either human or animals use.

Funding sources

This work was supported by the European Union - NextGenerationEU Call PRIN2022 Development of a plasmonic nanobiosensor for the rapid diagnosis of Shiga toxin producing E. coli human infections at the point of care - SENSOSTEC (CUP B53D23019990006).

Declaration of competing interest

The authors declare that they have no known competing financial

interests or personal relationships that could have appeared to influence the work reported in this paper.

Glossary

- •SERS Surface-enhanced Raman spectroscopy - a technique that amplifies Raman scattering using plasmonic nanostructures, enabling ultrasensitive molecular detection
- •Kapton a flexible polyimide tape fabricated for the first time by Dupont
- •Stx Shiga toxin - a potent bacterial toxin responsible for severe gastrointestinal and systemic diseases in humans
- •STEC Shiga toxin-producing Escherichia coli - pathogenic strains of E. coli that produce Shiga toxins
- •HUS: Hemolytic uremic syndrome - a life-threatening condition characterized by hemolytic anemia, thrombocytopenia, and acute kidney injury
- •EF Enhancement Factor - a metric quantifying the amplification of Raman signals in SERS relative to conventional Raman
- •LOD Limit of detection - the lowest concentration of an analyte that can be reliably distinguished from background noise.
- •PBS Phosphate-buffered saline - a water-based salt solution used to maintain pH and osmolarity in biological experiments
- •$HAuCl_4 \cdot 3H_2O$ Hydrogen tetrachloroaurate(III) trihydrate a gold salt used as precursor for gold nanoparticle synthesis
- •$Na_3C_6H_5O_7 \cdot 2H_2O$ Trisodium citrate dihydrate a reducing and stabilizing agent for nanoparticle synthesis
- •4MBA 4-Mercaptobenzoic acid - a common Raman probe molecule used to evaluate the enhancement capabilities of SERS substrates due to its well-defined vibrational features
- •Langmuir–Blodgett technique method to assemble nanoparticle monolayers at liquid interfaces
- •Marangoni effect Interfacial tension-driven flow facilitating nanoparticle assembly at liquid interfaces
- •SEM Scanning electron microscopy - high-resolution imaging technique used to characterize nanostructures
- •RSD Relative Standard Deviation - statistical measure of signal reproducibility or variability across multiple SERS measurements, expressed as a percentage of the mean signal
- •LSPR Localized surface plasmon resonance – A phenomenon where conduction electrons in metal nanoparticles resonate with incident light, enhancing local electromagnetic fields; fundamental to SERS signal amplification
- •SPRi Surface plasmon resonance imaging – A label-free optical technique used to monitor biomolecular interactions in real time by detecting changes in refractive index near a metal surface
- •ELISA Enzyme-linked immunosorbent assay – A widely used biochemical method for detecting and quantifying specific proteins, antigens, or antibodies through enzyme-mediated colorimetric readouts
- •PCR Polymerase chain reaction – A molecular biology technique that amplifies specific DNA sequences, allowing sensitive and specific detection of genetic material from pathogens
- •PCA Principal component analysis - a statistical method used to reduce data dimensionality and identify patterns in complex datasets
- •K-means clustering unsupervised machine learning algorithm for grouping similar data points
- •ANOVA Analysis of variance, statistical method to assess differences between group means

Appendix A. Supplementary data

Supplementary data to this article can be found online at https://doi.org/10.1016/j.biosx.2025.100696.

Data availability

The datasets generated and/or analyzed during the current study are available from the corresponding author upon reasonable request.

References

Ahmed, S.R., Kim, J., Tran, V.T., Suzuki, T., Neethirajan, S., Lee, J., Park, E.Y., 2017. In situ self-assembly of gold nanoparticles on hydrophilic and hydrophobic substrates for influenza virus-sensing platform. Sci. Rep. 7. https://doi.org/10.1038/srep44495.

Aitekenov, S., Sultangaziyev, A., Ilyas, A., Dyussupova, A., Boranova, A., Gaipov, A., Bukasov, R., 2022. Surface-enhanced Raman spectroscopy (SERS) for protein determination in human urine. Sens. Biosens. Res. 38. https://doi.org/10.1016/j.sbsr.2022.100535.

Ardissino, G., Possenti, I., Vignati, C., Daprai, L., Capone, V., Brigotti, M., Luini, M.V., Consonni, D., Montini, G., n.d. Is Shigatoxin 1 protective for the development of Shigatoxin 2-related hemolytic uremic syndrome in children? Data from the ItalKid-HUS Network. https://doi.org/10.1007/s00467-020-04697-y/Published.

Arfilli, V., Carnicelli, D., Ardissino, G., Torresani, E., Scavia, G., Brigotti, M., 2015. A rapid and sensitive method to measure the functional activity of shiga toxins in human serum. Toxins (Basel) 7, 4564–4576. https://doi.org/10.3390/toxins7114564.

Armstrong, C.M., Ruth, L.E., Capobianco, J.A., Strobaugh, T.P., Rubio, F.M., Gehring, A. G., 2018. Detection of shiga toxin 2 produced by escherichia coli in foods using a novel AlphaLISA. Toxins (Basel) 10. https://doi.org/10.3390/toxins10110422.

Ataman, C., Kinkeldei, T., Mattana, G., Vásquez Quintero, A., Molina-Lopez, F., Courbat, J., Cherenack, K., Briand, D., Tröster, G., De Rooij, N.F., 2013. A robust platform for textile integrated gas sensors. Sensor. Actuator. B Chem. 177, 1053–1061. https://doi.org/10.1016/j.snb.2012.11.099.

Atta, S., Vo-Dinh, T., 2023. Solution-based ultra-sensitive surface-enhanced Raman scattering detection of the toxin bacterial biomarker pyocyanin in biological fluids using sharp-branched gold nanostars. Anal. Chem. 95, 2690–2697. https://doi.org/10.1021/acs.analchem.2c03210.

Bai, F., Dong, J., Qu, J., Zhang, Z., 2021. Construction of flexible, transparent and mechanically robust SERS-active substrate with an efficient spin coating method for rapid in-situ target molecules detection. Nanotechnology 32. https://doi.org/10.1088/1361-6528/ac09ab.

Barhoumi, A., Halas, N.J., 2010. Label-free detection of DNA hybridization using surface enhanced Raman spectroscopy. J. Am. Chem. Soc. 132, 12792–12793. https://doi.org/10.1021/ja105678z.

Beeram, R., Banerjee, D., Narlagiri, L.M., Soma, V.R., 2022. Machine learning for rapid quantification of trace analyte molecules using SERS and flexible plasmonic paper substrates. Anal. Methods. https://doi.org/10.1039/d2ay00408a.

Benson, K, S.W.S., Pitzer, W.P., Jencks, J., Carriuolo, J.F., Kirsch, W.P., Jencks, T.G., Bruice, U.K., Pandit, N.L., Allinger, J.T., Sprague, S., Kabuss, H., Friebolin, H., Schmid, L.M., Jackman, S., Sternhell, M.W., Hunkapiller, S., 1967. Applications of nuclear magnetic res-onance spectroscopy in organic chemistry. J. Am. Chem. Soc. Pergamon Press. Hulsgen and D. Ott.

Bhattacharya, S., Agarwal, A.K., Prakash, O., Singh, S., n.d. Sensors for automotive and aerospace applications energy, environment, and Sustainability Series Editors: Avinash Kumar Agarwal · Ashok Pandey.

Binnwei, D., n.d. Microsystems and Nanosystems Advanced Mechatronics and MEMS Devices II.

Biswas, S., Devi, Y.D., Sarma, D., Hatiboruah, D., Chamuah, N., Namsa, N.D., Nath, P., 2023a. Detection and analysis of rotavirus in clinical stool samples using silver nanoparticle functionalized paper as SERS substrate. Spectrochim. Acta Mol. Biomol. Spectrosc. 295. https://doi.org/10.1016/j.saa.2023.122610.

Biswas, S., Devi, Y.D., Sarma, D., Hatiboruah, D., Chamuah, N., Namsa, N.D., Nath, P., 2023b. Detection and analysis of rotavirus in clinical stool samples using silver nanoparticle functionalized paper as SERS substrate. Spectrochim. Acta Mol. Biomol. Spectrosc. 295. https://doi.org/10.1016/j.saa.2023.122610.

Botti, S., Rufoloni, A., Rindzevicius, T., Schmidt, M.S., 2018. Surface-enhanced Raman spectroscopy characterization of pristine and functionalized carbon nanotubes and graphene. In: Raman Spectroscopy. InTech. https://doi.org/10.5772/intechopen.74065.

Brandon, E.J., Vozoff, M., Kolawa, E.A., Studor, G.F., Lyons, F., Keller, M.W., Beiermann, B., White, S.R., Sottos, N.R., Curry, M.A., Banks, D.L., Brocato, R., Zhou, L., Jung, S., Jackson, T.N., Champaigne, K., 2011. Structural health management technologies for inflatable/deployable structures: integrating sensing and self-healing. Acta Astronaut. 68, 883–903. https://doi.org/10.1016/j.actaastro.2010.08.016.

Brigotti, M., Tazzari, P.L., Ravanelli, E., Carnicelli, D., Rocchi, L., Arfilli, V., Scavia, G., Minelli, F., Ricci, F., Pagliaro, P., Ferretti, A.V.S., Pecoraro, C., Paglialonga, F., Edefonti, A., Procaccino, M.A., Tozzi, A.E., Caprioli, A., 2011. Clinical relevance of shiga toxin concentrations in the blood of patients with hemolytic uremic syndrome. Pediatr. Infect. Dis. J. 30, 486–490. https://doi.org/10.1097/INF.0b013e3182074d22.

Brigotti, M., Orth-Höller, D., Carnicelli, D., Porcellini, E., Galassi, E., Tazzari, P.L., Ricci, F., Manoli, F., Manet, I., Talasz, H., Lindner, H.H., Speth, C., Erbeznik, T., Fuchs, S., Posch, W., Chatterjee, S., Würzner, R., 2019a. The structure of the Shiga toxin 2a A-subunit dictates the interactions of the toxin with blood components. Cell. Microbiol. 21. https://doi.org/10.1111/cmi.13000.

Brigotti, M., Orth-Höller, D., Carnicelli, D., Porcellini, E., Galassi, E., Tazzari, P.L., Ricci, F., Manoli, F., Manet, I., Talasz, H., Lindner, H.H., Speth, C., Erbeznik, T., Fuchs, S., Posch, W., Chatterjee, S., Würzner, R., 2019b. The structure of the Shiga toxin 2a A-subunit dictates the interactions of the toxin with blood components. Cell. Microbiol. 21. https://doi.org/10.1111/cmi.13000.

Brigotti, M., Orth-Höller, D., Carnicelli, D., Porcellini, E., Galassi, E., Tazzari, P.L., Ricci, F., Manoli, F., Manet, I., Talasz, H., Lindner, H.H., Speth, C., Erbeznik, T., Fuchs, S., Posch, W., Chatterjee, S., Würzner, R., 2019c. The structure of the Shiga toxin 2a A-subunit dictates the interactions of the toxin with blood components. Cell. Microbiol. 21. https://doi.org/10.1111/cmi.13000.

Brown, P.I., Ojiakor, A., Chemello, A.J., Fowler, C.C., 2023. The diverse landscape of AB5-type toxins. Eng. Microbiol. https://doi.org/10.1016/j.engmic.2023.100104.

Caillard, L., Seitz, O., Campbell, P.M., Doherty, R.P., Lamic-Humblot, A.F., Lacaze, E., Chabal, Y.J., Pluchery, O., 2013. Gold nanoparticles on oxide-free silicon-molecule interface for single electron transport. Langmuir 29, 5066–5073. https://doi.org/10.1021/la304971v.

Canning, A.J., Li, J.Q., Atta, S., Wang, H.N., Vo-Dinh, T., 2024. Nanoplasmonics biosensors: at the frontiers of biomedical diagnostics. TrAC, Trends Anal. Chem. https://doi.org/10.1016/j.trac.2024.117973.

Chang, R., Wang, T., Liu, Q., Tang, J., Wu, D., 2022. Ag Nanoparticles@Agar gel as a 3D flexible and stable SERS substrate with ultrahigh sensitivity. Langmuir 38, 13822–13832. https://doi.org/10.1021/acs.langmuir.2c01966.

Chen, C.M., Lord, R.C., 1976. Laser-Excited Raman spectroscopy of biomolecules. VIII. Conformational study of bovine serum album. J. Am. Chem. Soc. Pergamon Press. https://doi.org/10.1021/ja00420a021. Hulsgen and D. Ott.

Chen, D., Zhou, J., Rippa, M., Petti, L., 2015. Structure-dependent localized surface plasmon resonance characteristics and surface enhanced Raman scattering performances of quasi-periodic nanoarrays: measurements and analysis. J. Appl. Phys. 118. https://doi.org/10.1063/1.4934490.

Chen, W., Gui, X., Zheng, Y., Liang, B., Lin, Z., Zhao, C., Chen, H., Chen, Z., Li, X., Tang, Z., 2017. Synergistic effects of wrinkled graphene and plasmonics in stretchable hybrid platform for surface-enhanced Raman spectroscopy. Adv. Opt. Mater. 5. https://doi.org/10.1002/adom.201600715.

Chen, L., Ying, B., Song, P., Liu, X., 2019. A nanocellulose-paper-based SERS multiwell plate with high sensitivity and high signal homogeneity. Adv. Mater. Interfac. 6. https://doi.org/10.1002/admi.201901346.

Chen, Z., Sun, Y., Zhang, X., Shen, Y., Khalifa, S.A.M., Huang, X., Shi, J., Li, Z., Zou, X., 2024. Green and sustainable self-cleaning flexible SERS base: utilized for cyclic-detection of residues on apple surface. Food Chem. 441. https://doi.org/10.1016/j.foodchem.2023.138345.

Chou, I.H., Benford, M., Beier, H.T., Coté, G.L., Wang, M., Jing, N., Kameoka, J., Good, T. A., 2008. Nanofluidic biosensing for β-amyloid detection using surface enhanced Raman spectroscopy. Nano Lett. 8, 1729–1735. https://doi.org/10.1021/nl0808132.

Ditta, A., Zhang, R., Nawaz, H., Majeed, M.I., He, S., Zhuang, Z., Rütten, S., Shahzadi, A., Yaseen, S., Kiessling, F., Hu, J., Lammers, T., Pallares, R.M., 2025. An exploratory clinical study of the diagnosis and staging of typhoid fever using label-free surface-enhanced Raman spectroscopy liquid biopsy. Spectrochim. Acta Mol. Biomol. Spectrosc. 333. https://doi.org/10.1016/j.saa.2025.125864.

Fazio, B., D'Andrea, C., Foti, A., Messina, E., Irrera, A., Donato, M.G., Villari, V., Micali, N., Maragò, O.M., Gucciardi, P.G., 2016. SERS detection of biomolecules at physiological pH via aggregation of gold nanorods mediated by optical forces and plasmonic heating. Sci. Rep. 6. https://doi.org/10.1038/srep26952.

Fraser, M.E., Fujinaga, M., Cherney, M.M., Melton-Celsa, A.R., Twiddy, E.M., O'Brien, A. D., James, M.N.G., 2004. Structure of shiga toxin type 2 (Stx2) from Escherichia coli O157:H7. J. Biol. Chem. 279, 27511–27517. https://doi.org/10.1074/jbc.M401939200.

Freedman, S.B., van de Kar, N.C.A.J., Tarr, P.I., 2023. Shiga toxin–producing Escherichia coli and the hemolytic–uremic syndrome. N. Engl. J. Med. 389, 1402–1414. https://doi.org/10.1056/nejmra2108739.

Georgiev, P., Bojinova, A., Kostova, B., Momekova, D., Bjornholm, T., Balashev, K., 2013. Implementing atomic force microscopy (AFM) for studying kinetics of gold nanoparticle's growth. Colloids Surf. A Physicochem. Eng. Asp. 434, 154–163. https://doi.org/10.1016/j.colsurfa.2013.05.064.

Giménez, M.C., Del Pópolo, M.G., Leiva, E.P.M., García, S.G., Salinas, D.R., Mayer, C.E., Lorenz, W.J., 2002. Theoretical Considerations of Electrochemical Phase Formation for an Ideal Frank-van der Merwe System. J. Electrochem. Soc. 149, E109. https://doi.org/10.1149/1.1457986.

Goel, R., Chakraborty, S., Awasthi, V., Bhardwaj, V., Kumar Dubey, S., 2024. Exploring the various aspects of Surface enhanced Raman spectroscopy (SERS) with focus on the recent progress: SERS-active substrate, SERS-instrumentation, SERS-application. Sens. Actuators A Phys. https://doi.org/10.1016/j.sna.2024.115555.

Grzelczak, M., Pérez-Juste, J., Mulvaney, P., Liz-Marzán, L.M., 2008. Shape control in gold nanoparticle synthesis. Chem. Soc. Rev. 37, 1783–1791. https://doi.org/10.1039/b711490g.

Hameed, S., Xie, L., Ying, Y., 2018. Conventional and emerging detection techniques for pathogenic bacteria in food science: a review. Trends Food Sci. Technol. https://doi.org/10.1016/j.tifs.2018.05.020.

Hamm, L., Gee, A., Indrasekara, A.S.D.S., 2019. Recent advancement in the surface-enhanced Raman spectroscopy-based biosensors for infectious disease diagnosis. Appl. Sci.(Switzerland). https://doi.org/10.3390/app9071448.

Han, D., Guo, B., Li, Y., Feng, W., Liu, K., Wu, T., Wan, Y., Wang, L., Gao, M., Liu, Y., Yang, L., Wei, M., Yang, S., 2024. Simultaneous photocatalytic degradation and SERS detection of tetracycline with self-sustainable and recyclable ternary PI/TiO2/Ag flexible microfibers. Microsyst. Nanoeng. 10. https://doi.org/10.1038/s41378-023-00624-x.

Haque Chowdhury, M.A., Tasnim, N., Hossain, M., Habib, A., 2023. Flexible, stretchable, and single-molecule-sensitive SERS-active sensor for wearable biosensing applications. RSC Adv. 13, 20787–20798. https://doi.org/10.1039/d3ra03050d.

He, P., Mehedi Hassan, M., Yang, W., Shi, Z., Zhou, X., Xu, Y., Ouyang, Q., Chen, Q., 2023a. Rapid and stable detection of three main mycotoxins in rice using SERS optimized AgNPs@K30 coupled multivariate calibration. Food Chem. 398. https://doi.org/10.1016/j.foodchem.2022.133883.

He, P., Mehedi Hassan, M., Yang, W., Shi, Z., Zhou, X., Xu, Y., Ouyang, Q., Chen, Q., 2023b. Rapid and stable detection of three main mycotoxins in rice using SERS optimized AgNPs@K30 coupled multivariate calibration. Food Chem. 398. https://doi.org/10.1016/j.foodchem.2022.133883.

Hosny, M., Wissem, D., Ikbel, H., Hatem, E., 2014. Influence of gold nanoparticles deposition on porous silicon properties. Sens. Transducers.

Huang, J.A., Mousavi, M.Z., Giovannini, G., Zhao, Y., Hubarevich, A., Soler, M.A., Rocchia, W., Garoli, D., De Angelis, F., 2020. Multiplexed discrimination of single amino acid residues in polypeptides in a single SERS hot spot. Angew. Chem. Int. Ed. 59, 11423–11431. https://doi.org/10.1002/anie.202000489.

Hwang, J., Lee, S., Choo, J., 2016. Application of a SERS-based lateral flow immunoassay strip for the rapid and sensitive detection of staphylococcal enterotoxin B. Nanoscale 8, 11418–11425. https://doi.org/10.1039/c5nr07243c.

Ikotun, A.M., Ezugwu, A.E., Abualigah, L., Abuhaija, B., Heming, J., 2023. K-means clustering algorithms: a comprehensive review, variants analysis, and advances in the era of big data. Inf Sci (N Y) 622, 178–210. https://doi.org/10.1016/j.ins.2022.11.139.

Ilyas, A., Dyussupova, A., Sultangaziyev, A., Shevchenko, Y., Filchakova, O., Bukasov, R., 2023. SERS immuno- and apta-assays in biosensing/bio-detection: performance comparison, clinical applications, challenges. Talanta. https://doi.org/10.1016/j.talanta.2023.124818.

Islam, M.K., Ali, M.S., Miah, M.S., Rahman, M.M., Alam, M.S., Hossain, M.A., 2021. Brain tumor detection in MR image using superpixels, principal component analysis and template based K-means clustering algorithm. Machine Learning Appl. 5, 100044. https://doi.org/10.1016/j.mlwa.2021.100044.

Jess, P.R.T., Smith, D.D.W., Mazilu, M., Dholakia, K., Riches, A.C., Herrington, C.S., 2007. Early detection of cervical neoplasia by Raman spectroscopy. Int. J. Cancer 121, 2723–2728. https://doi.org/10.1002/ijc.23046.

Jiang, X., Lillehoj, P.B., 2020. Microneedle-based skin patch for blood-free rapid diagnostic testing. Microsyst. Nanoeng. 6. https://doi.org/10.1038/s41378-020-00206-1.

Jiang, H., Manolache, S., Wong, A.C.L., Denes, F.S., 2004. Plasma-enhanced deposition of silver nanoparticles onto polymer and metal surfaces for the generation of antimicrobial characteristics. J. Appl. Polym. Sci. 93, 1411–1422. https://doi.org/10.1002/app.20561.

Jiang, X., Li, K., Tang, Y., Wang, X., Kan, W., Yang, L., Zhao, B., 2024. A double defects-dominated flexible TiO2 matrix for in-situ SERS sensing of antibiotic residues in aquatic ecosystem (fish & fishpond water) and their on-site degradation in flowing water. Sci. Total Environ. 921. https://doi.org/10.1016/j.scitotenv.2024.171154.

Dong, Jun, 2023. Y.C.J.Y.H.W.Y.Z.C.L.Q.H.W.G.Y.W. and J.Q. Low-cost and Flexible Paper-Based Plasmonic Nanostructure for a Highly Sensitive SERS Substrate.

Kadam, U.S., Hong, J.C., 2022. Advances in aptameric biosensors designed to detect toxic contaminants from food, water, human fluids, and the environment. Trends in Environment. Analytical Chem. https://doi.org/10.1016/j.teac.2022.e00184.

Kang, H., Heo, C.J., Jeon, H.C., Lee, S.Y., Yang, S.M., 2013. Durable plasmonic cap arrays on flexible substrate with real-time optical tunability for high-fidelity SERS devices. ACS Appl. Mater. Interfaces 5, 4569–4574. https://doi.org/10.1021/am400019v.

Karbalaee, Z., Rezayan, A.H., Taheri, R.A., Mirhosseini, S.A., Barshan-Tashnizi, M., 2025. Enhancing Shiga toxin detection using surface plasmon resonance a study of antibody immobilization strategies. Sci. Rep. 15, 17024. https://doi.org/10.1038/s41598-025-01686-9.

Kim, W., Kim, Y.H., Park, H.K., Choi, S., 2015. Facile fabrication of a silver nanoparticle immersed, surface-enhanced Raman scattering imposed paper platform through successive ionic layer absorption and reaction for on-site bioassays. ACS Appl. Mater. Interfaces 7, 27910–27917. https://doi.org/10.1021/acsami.5b09982.

Kimura, K., Kobayashi, K., Matsushige, K., Yamada, H., 2013. Imaging of Au nanoparticles deeply buried in polymer matrix by various atomic force microscopy techniques. Ultramicroscopy 133, 41–49. https://doi.org/10.1016/j.ultramic.2013.04.003.

Koutsoumanis, K., Allende, A., Alvarez-Ordóñez, A., Bover-Cid, S., Chemaly, M., Davies, R., De Cesare, A., Herman, L., Hilbert, F., Lindqvist, R., Nauta, M., Peixe, L., Ru, G., Simmons, M., Skandamis, P., Suffredini, E., Jenkins, C., Monteiro Pires, S., Morabito, S., Niskanen, T., Scheutz, F., da Silva Felício, M.T., Messens, W., Bolton, D., 2020. Pathogenicity assessment of Shiga toxin-producing Escherichia coli (STEC) and the public health risk posed by contamination of food with STEC. EFSA J. 18. https://doi.org/10.2903/j.efsa.2020.5967.

Kudelski, A., 2005. Characterization of thiolate-based mono- and bilayers by vibrational spectroscopy: a review. Vib. Spectrosc. 39, 200–213. https://doi.org/10.1016/j.vibspec.2005.03.005.

Kumar, S., Goel, P., Singh, J.P., 2017. Flexible and robust SERS active substrates for conformal rapid detection of pesticide residues from fruits. Sensor. Actuator. B Chem. 241, 577–583. https://doi.org/10.1016/j.snb.2016.10.106.

Lahokallio, S., Kiilunen, J., Frisk, L., 2014. High temperature reliability of electrically conductive adhesive attached temperature sensors on flexible polyimide substrates. In: Microelectronics Reliability. Elsevier Ltd, pp. 2017–2022. https://doi.org/10.1016/j.microrel.2014.07.095.

Lai, W., Zhou, J., Jia, Z., Petti, L., Mormile, P., 2015. Ag@Au hexagonal nanorings: synthesis, mechanistic analysis and structure-dependent optical characteristics. J. Mater Chem. C Mater. 3, 9726–9733. https://doi.org/10.1039/c5tc02017d.

Lee, C.H., Hankus, M.E., Tian, L., Pellegrino, P.M., Singamaneni, S., 2011. Highly sensitive surface enhanced Raman scattering substrates based on filter paper loaded with plasmonic nanostructures. Anal. Chem. 83, 8953–8958. https://doi.org/10.1021/ac2016882.

Li, H., Zhang, H., Luo, W., Yuan, R., Zhao, Y., Huang, J.A., Yang, X., 2022. Microcontact printing of gold nanoparticle at three-phase interface as flexible substrate for SERS detection of MicroRNA. Anal. Chim. Acta 1229. https://doi.org/10.1016/j.aca.2022.340380.

Liang, L., Zhao, X., Wen, J., Liu, J., Zhang, F., Guo, X., Zhang, K., Wang, A., Gao, R., Wang, Y., Zhang, Y., 2022. Flexible SERS substrate with a Ag-SiO2Cosputtered film for the rapid and convenient detection of thiram. Langmuir 38, 13753–13762. https://doi.org/10.1021/acs.langmuir.2c01853.

Lim, J.M., Heo, N.S., Oh, S.Y., Ryu, M.Y., Seo, J.H., Park, T.J., Huh, Y.S., Park, J.P., 2018. Selection of affinity peptides for interference-free detection of cholera toxin. Biosens. Bioelectron. 99, 289–295. https://doi.org/10.1016/j.bios.2017.07.075.

Lim, C.Y., Granger, J.H., Porter, M.D., 2019. SERS detection of Clostridium botulinum neurotoxin serotypes A and B in buffer and serum: towards the development of a biodefense test platform. Anal. Chim. Acta X, 1. https://doi.org/10.1016/j.acax.2018.100002.

Lin, V.J.C., Koenig, J.L., 1976a. Raman studies of bovine serum albumin. Biopolymers 15, 203–218. https://doi.org/10.1002/bip.1976.360150114.

Lin, V.J.C., Koenig, J.L., 1976b. Raman studies of bovine serum albumin. Biopolymers 15, 203–218. https://doi.org/10.1002/bip.1976.360150114.

Lin, X., Fang, G., Liu, Y., He, Y., Wang, L., Dong, B., 2020. Marangoni effect-driven transfer and compression at three-phase interfaces for highly reproducible nanoparticle monolayers. J. Phys. Chem. Lett. 11, 3573–3581. https://doi.org/10.1021/acs.jpclett.0c01116.

Lin, L.K., Tsai, J.T., Dã-Az-Amaya, S., Oduncu, M.R., Zhang, Y., Huang, P.Y., Ostos, C., Schmelzel, J.P., Mohammadrahimi, R., Xu, P., Ulloa Gomez, A.M., Shuvo, S.N., Raghunathan, N., Zhang, X., Wei, A., Bahr, D., Peroulis, D., Stanciu, L.A., 2021. Antidelaminating, thermally stable, and cost-effective flexible kapton platforms for nitrate sensors, mercury aptasensors, protein sensors, and p-type organic thin-film transistors. ACS Appl. Mater. Interfaces 13, 11369–11384. https://doi.org/10.1021/acsami.0c18426.

Liu, R., Jiang, L., Yu, Z., Chen, Y., Xu, R., Jin, S., 2020. Flexible SERS Platform Based on Ti3C2Tx-Modified Filter Paper: Preparation and SERS Application. Appl Opt. 59 (26), 7846–7852. https://doi.org/10.1364/AO.398454.

Liu, X., Ma, J., Jiang, P., Shen, J., Wang, R., Wang, Y., Tu, G., 2020a. Large-scale flexible surface-enhanced Raman scattering (SERS) sensors with high stability and signal homogeneity. ACS Appl. Mater. Interfaces 12, 45332–45341. https://doi.org/10.1021/acsami.0c13691.

Liu, X., Ma, J., Jiang, P., Shen, J., Wang, R., Wang, Y., Tu, G., 2020b. Large-scale flexible surface-enhanced Raman scattering (SERS) sensors with high stability and signal homogeneity. ACS Appl. Mater. Interfaces 12, 45332–45341. https://doi.org/10.1021/acsami.0c13691.

Loxd, R.C., Yu, N.-T., 1970. Laser-excited Raman spectroscopy of biomolecules I. Native lysozyme and its constituent amino acids. J. Mol. Biol.

Lu, T., Zhu, K. Di, Huang, C., Wen, T., Jiao, Y.J., Zhu, J., Zhang, Q., Ding, S.N., 2020. Rapid detection of Shiga toxin type II using lateral flow immunochromatography test strips of colorimetry and fluorimetry. Analyst 145, 76–82. https://doi.org/10.1039/c9an01996k.

Ma, X., Xie, J., Wang, Z., Zhang, Y., 2022. Transparent and flexible AuNSs/PDMS-based SERS substrates for in-situ detection of pesticide residues. Spectrochim. Acta Mol. Biomol. Spectrosc. 267. https://doi.org/10.1016/j.saa.2021.120542.

Ma, Y., Xia, S., Hu, A., Zhang, Q., Shao, Z., Tian, B., Lin, Q., 2025. Ultrabright contrast agents with synergistic Raman enhancements for precise intraoperative imaging and photothermal ablation of orthotopic tumor models. J. Nanobiotechnol. 23, 26. https://doi.org/10.1186/s12951-025-03099-2.

Madani, M., Heydari, Z., Poursafar, J., Sharifpour, N., Kolahdouz, M., Asl-Soleimani, E., Aghababa, H., 2024. A study of kapton as a flexible substrate for perovskite solar cells; advantages and disadvantages. Opt. Mater. 154. https://doi.org/10.1016/j.optmat.2024.115697.

Madzharova, F., Heiner, Z., Gühlke, M., Kneipp, J., 2016. Surface-enhanced hyper-Raman spectra of adenine, guanine, cytosine, thymine, and uracil. J. Phys. Chem. C 120, 15415–15423. https://doi.org/10.1021/acs.jpcc.6b02753.

Martiny, N., Rheinfeld, A., Geder, J., Wang, Y., Kraus, W., Jossen, A., 2014. Development of an all kapton-based thin-film thermocouple matrix for in situ temperature measurement in a lithium ion pouch cell. IEEE Sens. J. 14, 3377–3384. https://doi.org/10.1109/JSEN.2014.2331996.

Matussek, A., Lauber, J., Bergau, A., Hansen, W., Rohde, M., Dittmar, K.E.J., Gunzer, M., Mengel, M., Gatzlaff, P., Hartmann, M., Buer, J., Gunzer, F., 2003. Molecular and functional analysis of Shiga toxin-induced response patterns in human vascular endothelial cells. Blood 102, 1323–1332. https://doi.org/10.1182/blood-2002-10-3301.

Maurizio, Brigotti, 2020. Particulate shiga toxin 2 in blood is associated to the development of hemolytic uremic syndrome in children. Thromb. Haemost.

McDonnell, C., Albarghouthi, F.M., Selhorst, R., Kelley-Loughnane, N., Franklin, A.D., Rao, R., 2023a. Aerosol jet printed surface-enhanced Raman substrates: application for high-sensitivity detection of perfluoroalkyl substances. ACS Omega 8, 1597–1605. https://doi.org/10.1021/acsomega.2c07134.

McDonnell, C., Albarghouthi, F.M., Selhorst, R., Kelley-Loughnane, N., Franklin, A.D., Rao, R., 2023b. Aerosol jet printed surface-enhanced Raman substrates: application for high-sensitivity detection of perfluoroalkyl substances. ACS Omega 8, 1597–1605. https://doi.org/10.1021/acsomega.2c07134.

Melinte, V., Radu, A.M., Văcăroiu, C.M., Cismaru, M.I., Oprescu Macovei, A.M., Mihăilă, D.E., Gheorghiță, V., 2024. A successful approach to diagnosing shiga-like toxin-producing Escherichia coli-induced colitis. Diagnostics 14. https://doi.org/10.3390/diagnostics14080801.

Menge, C., 2020. Toxins molecular biology of Escherichia coli shiga toxins'. Effects on Mammalian Cells. https://doi.org/10.3390/toxins12060345.

Metal Nanoparticles On Polymer Surfaces 747 (1), 2001.

Mirhosseini, S.A., Sedighian, H., Amani, J., Behzadi, E., Fooladi, A.A.I., 2022. Detection of some enteric bacterial toxin via modified ELISA assay. J. Appl. Biotechnol. Rep. 9, 622–631. https://doi.org/10.30491/jabr.2020.227628.1214.

Mocák, J., Janiga, I., Rábarová, E., 2009. EVALUATION OF IUPAC LIMIT OF DETECTION AND ISO MINIMUM DETECTABLE VALUE-ELECTROCHEMICAL DETERMINATION OF LEAD. Nova Biotechnologica.

Nagatsuka, T., Uzawa, H., Sato, K., Kondo, S., Izumi, M., Yokoyama, K., Ohsawa, I., Seto, Y., Neri, P., Mori, H., Nishida, Y., Saito, M., Tamiya, E., 2013. Localized surface plasmon resonance detection of biological toxins using cell surface oligosaccharides on glyco chips. ACS Appl. Mater. Interfaces 5, 4173–4180. https://doi.org/10.1021/am4002937.

Nakamura, K., Era, S., Ozaki, Y., Sogami, M., Hayashi, T., Murakami, M., 1997. Conformational changes in seventeen cystine disulfide bridges of bovine serum albumin proved by Raman spectroscopy. FEBS Lett. 417, 375–378. https://doi.org/10.1016/S0014-5793(97)01326-4.

Negri, P., Schultz, Z.D., 2014. Online SERS detection of the 20 proteinogenic L-amino acids separated by capillary zone electrophoresis. Analyst 139, 5989–5998. https://doi.org/10.1039/c4an01177e.

Nguyen, H.A., Mai, Q.D., Nguyet Nga, D.T., Pham, M.K., Nguyen, Q.K., Do, T.H., Luong, V.T., Lam, V.D., Le, A.T., 2024. Paper/GO/e-Au flexible SERS sensors for in situ detection of tricyclazole in orange juice and on cucumber skin at the sub-ppb level: machine learning-assisted data analysis. Nanoscale Adv. 6, 3106–3118. https://doi.org/10.1039/d3na01113e.

Palermo, G., Rippa, M., Conti, Y., Vestri, A., Castagna, R., Fusco, G., Suffredini, E., Zhou, J., Zyss, J., De Luca, A., Petti, L., 2021. Plasmonic metasurfaces based on pyramidal nanoholes for high-efficiency SERS biosensing. ACS Appl. Mater. Interfaces 13, 43715–43725. https://doi.org/10.1021/acsami.1c12525.

Palermo, G., Rippa, M., Aceti, D.M., Guglielmelli, A., Valente, L., Sagnelli, D., D'Avino, A., Guilcapi, B., Maccaferri, N., Petti, L., Strangi, G., 2024. Intrinsic superchirality in planar plasmonic metasurfaces. Nano Lett. 24, 10202–10209. https://doi.org/10.1021/acs.nanolett.4c02530.

Pan, Y., Xu, S., Wang, Z., Jiang, C., Ma, X., 2024. Sensitive SERS aptasensor for histamine detection based on Au/Ag nanorods and IRMOF-3@Au based flexible PDMS membrane. Anal. Chim. Acta 1288. https://doi.org/10.1016/j.aca.2023.342147.

Pang, C., Lee, C., Suh, K.Y., 2013. Recent advances in flexible sensors for wearable and implantable devices. J. Appl. Polym. Sci. https://doi.org/10.1002/app.39461.

Park, S., Lee, J., Ko, H., 2017. Transparent and flexible surface-enhanced Raman scattering (SERS) sensors based on gold nanostar arrays embedded in silicon rubber film. ACS Appl. Mater. Interfaces 9, 44088–44095. https://doi.org/10.1021/acsami.7b14022.

Peng, S., Zhang, Z., Guo, J., Ma, T., Liu, D., 2025. Rapid detection of thiram on apple surfaces using a flexible and sticky SERS substrate coupled with chemometric methods. Spectrochim. Acta Mol. Biomol. Spectrosc. 328. https://doi.org/10.1016/j.saa.2024.125435.

Pham, A.T., Bui, H.N., Mai, Q.D., Le, A.T., 2023. Flexible, high-performance and facile PVA/cellulose/Ag SERS chips for in-situ and rapid detection of thiram pesticide in apple juice. Heliyon 9, e19926. https://doi.org/10.1016/j.heliyon.2023.e19926.

Phan, H.P., Dinh, T., Nguyen, T.K., Qamar, A., Nguyen, T., Dau, V.T., Han, J., Dao, D.V., Nguyen, N.T., 2020. High temperature silicon-carbide-based flexible electronics for monitoring hazardous environments. J. Hazard. Mater. 394. https://doi.org/10.1016/j.jhazmat.2020.122486.

Philip, R.M., Mohan, D.B., 2024. SERS and SE-FTIR platforms from plasmonic bismuth thin films for label-free multiplexed biomolecules detection. J. Mater. Sci. Mater. Electron. 35. https://doi.org/10.1007/s10854-024-13337-2.

Picone, A.L., Rizzato, M.L., Lusi, A.R., Romano, R.M., 2022. Stamplike flexible SERS substrate for in-situ rapid detection of thiram residues in fruits and vegetables. Food Chem. 373. https://doi.org/10.1016/j.foodchem.2021.131570.

Prakash, V., Rodriguez, R.D., Al-Hamry, A., Lipovka, A., Dorozhko, E., Selyshchev, O., Ma, B., Sharma, S., Mehta, S.K., Dzhagan, V., Mukherjee, A., Zahn, D.R.T., Kanoun, O., Sheremet, E., 2019. Flexible plasmonic graphene oxide/heterostructures for dual-channel detection. Analyst 144, 3297–3306. https://doi.org/10.1039/c8an02495b.

Qiu, H., Wang, M., Jiang, S., Zhang, L., Yang, Z., Li, L., Li, J., Cao, M., Huang, J., 2017. Reliable molecular trace-detection based on flexible SERS substrate of graphene/Ag-nanoflowers/PMMA. Sensor. Actuator. B Chem. 249, 439–450. https://doi.org/10.1016/j.snb.2017.04.118.

Ramezani Farani, M., Kim, H., Alhammadi, M., Huh, Y.S., 2024. The detection of toxic gases (CO, FN3, HI, N2, CH4, N2O, and O3) using a wearable Kapton–graphene biosensor for environmental and biomedical applications. Carbon Lett. https://doi.org/10.1007/s42823-024-00834-x.

Rezaei, I., Haghverdi, A.B., Soldoozy, A., Aghaee, T., Biabanifard, S., 2024. Wearable Kapton graphene biosensor for detection of toxic gases. J. Hazardous Mater.Adv. 15. https://doi.org/10.1016/j.hazadv.2024.100452.

Rippa, M., Castagna, R., Pannico, M., Musto, P., Borriello, G., Paradiso, R., Galiero, G., Censi, S.B., Zhou, J., Zyss, J., Petti, L., 2017. Octupolar metastructures for a highly sensitive, rapid, and reproducible phage-based detection of bacterial pathogens by surface-enhanced Raman scattering. ACS Sens. 2, 947–954. https://doi.org/10.1021/acssensors.7b00195.

Rippa, M., Sagnelli, D., Vestri, A., Marchesano, V., Munari, B., Carnicelli, D., Varrone, E., Brigotti, M., Tozzoli, R., Montalbano, M., Morabito, S., Zhou, J., Zyss, J., Petti, L.,

2022a. Plasmonic metasurfaces for specific SERS detection of shiga toxins. ACS Appl. Mater. Interfaces 14, 4969–4979. https://doi.org/10.1021/acsami.1c21553.
Rippa, M., Sagnelli, D., Vestri, A., Marchesano, V., Munari, B., Carnicelli, D., Varrone, E., Brigotti, M., Tozzoli, R., Montalbano, M., Morabito, S., Zhou, J., Zyss, J., Petti, L., 2022b. Plasmonic metasurfaces for specific SERS detection of shiga toxins. ACS Appl. Mater. Interfaces 14, 4969–4979. https://doi.org/10.1021/ACSAMI.1C21553.
Rippa, M., Sagnelli, D., Vestri, A., Marchesano, V., Munari, B., Carnicelli, D., Varrone, E., Brigotti, M., Tozzoli, R., Montalbano, M., Morabito, S., Zhou, J., Zyss, J., Petti, L., 2022c. Plasmonic metasurfaces for specific SERS detection of shiga toxins. ACS Appl. Mater. Interfaces 14, 4969–4979. https://doi.org/10.1021/acsami.1c21553.
Rippa, M., Marchesano, V., Vestri, A., Sagnelli, D., Fusco, G., Zyss, J., Lin, D., Zhou, J., Petti, L., 2024. Fractal plasmonic molecule for multi-sensing: SERS platform for SARS-CoV-2 detection. ACS Appl. Nano Mater. 7, 6958–6968. https://doi.org/10.1021/acsanm.3c06006.
Rippa, M., Milano, A., Marchesano, V., Sagnelli, D., Guilcapi, B., D'Avino, A., Palermo, G., Strangi, G., Consagra, L., Brigotti, M., Morabito, S., Zyss, J., Petti, L., 2025a. Diagnostic oriented discrimination of different Shiga toxins via PCA-assisted SERS-based plasmonic metasurface. Nanophotonics. https://doi.org/10.1515/nanoph-2024-0696.
Rippa, M., Milano, A., Marchesano, V., Sagnelli, D., Guilcapi, B., D'Avino, A., Palermo, G., Strangi, G., Consagra, L., Brigotti, M., Morabito, S., Zyss, J., Petti, L., 2025b. Diagnostic oriented discrimination of different Shiga toxins via PCA-assisted SERS-based plasmonic metasurface. Nanophotonics. https://doi.org/10.1515/nanoph-2024-0696.
Robert, A., Wiels, J., 2021. Shiga toxins as antitumor tools. Toxins (Basel). https://doi.org/10.3390/toxins13100690.
Rongyang, Liu, 2020. Flexible SERS Platform Based on Ti3C2Tx-Modified Filter Paper: Preparation and SERS Application. Appl Opt.
Ryd, M., Alfredsson, H., Blomberg, L., Andersson, Å., Lindberg, A.A., 1989. Purification of Shiga toxin by α-d-galactose-(1 → 4)-β-d-galactose-(1 → 4)- β-d-glucose-(1 →) receptor ligand-based chromatography. FEBS Lett. 258, 320–322. https://doi.org/10.1016/0014-5793(89)81684-9.
Seifi, M., Hamedi, S., Kordrostami, Z., 2022. Fabrication of a high-sensitive wearable temperature sensor with an improved response time based on PEDOT:PSS/rGO on a flexible kapton substrate. J. Mater. Sci. Mater. Electron. 33, 6954–6968. https://doi.org/10.1007/s10854-022-07875-w.
Shahid, U., Rashid, N., Javed, M.R., Majeed, M.I., Mohsin, M., Nawaz, H., Seemab, R., Zohaib, M., Alam, M., Alshammari, A., Albekairi, N.A., Shafique, H., Shahid, H., 2024. Surface-enhanced Raman spectroscopy for the rapid identification of fosfomycin resistant and sensitive strains of E. coli. Spectrochim. Acta Mol. Biomol. Spectrosc. 329, 125517. https://doi.org/10.1016/j.saa.2024.125517.
Shao, T., Xu, J., Zhong, H., Hu, Y., Chen, J., 2024a. A stable and flexible Au@Ag NPs/PVA SERS platform for thiram residue detection on rough surface. Talanta 274. https://doi.org/10.1016/j.talanta.2024.126008.
Shao, T., Xu, J., Zhong, H., Hu, Y., Chen, J., 2024b. A stable and flexible Au@Ag NPs/PVA SERS platform for thiram residue detection on rough surface. Talanta 274. https://doi.org/10.1016/j.talanta.2024.126008.
Sharma, V., Javed, B., Estrada, G., Byrne, H.J., Tian, F., 2024. In situ tuning and investigating the growth process of size controllable gold nanoparticles and statistical size prediction analysis. Colloids Surf. A Physicochem. Eng. Asp. 681. https://doi.org/10.1016/j.colsurfa.2023.132733.
Shrivastava, A., Gupta, V., 2011. Methods for the determination of limit of detection and limit of quantitation of the analytical methods. Chronicles Young Sci. 2, 21. https://doi.org/10.4103/2229-5186.79345.
Simeral, M.L., Zhang, A., Demers, S.M.E., Hughes, H.J., Abdul-Moqueet, M., Mayer, K.M., Hafner, J.H., 2021. Effects of conformational variation on structural insights from solution-phase surface-enhanced Raman spectroscopy. J. Phys. Chem. B 125, 2031–2041. https://doi.org/10.1021/acs.jpcb.0c10576.
Springer Browne, A., Midwinter, A.C., Withers, A.H., Cookson, A.L., Biggs, P.J., Marshall, J.C., Benschop, J., Hathaway, S., Rogers, L., Nisa, S., Hranac, C.R., Winkleman, T., French, N.P., 2021. Transmission dynamics of shiga toxin-producing Escherichia coli in New Zealand cattle from farm to slaughter. Appl. Environ. Microbiol. 87, 1–16. https://doi.org/10.1128/AEM.02907-20.
Srinivasan, K.P., Muthuramalingam, T., Elsheikh, A.H., 2023. A review of flexible printed sensors for automotive infotainment systems. Arch. Civ. Mech. Eng. https://doi.org/10.1007/s43452-023-00604-y.
Stearns-Kurosawa, D.J., Collins, V., Freeman, S., Tesh, V.L., Kurosawa, S., 2010. Distinct physiologic and inflammatory responses elicited in baboons after challenge with Shiga toxin type 1 or 2 from enterohemorrhagic Escherichia coli. Infect. Immun. 78, 2497–2504. https://doi.org/10.1128/IAI.01435-09.
Subekin, A., Alieva, R., Kukushkin, V., Oleynikov, I., Zavyalova, E., 2023. Rapid SERS detection of botulinum neurotoxin type A. Nanomaterials 13. https://doi.org/10.3390/nano13182531.
Suleimenova, A., Frasco, M.F., Sales, M.G.F., 2024. An ultrasensitive paper-based SERS sensor for detection of nucleolin using silver-nanostars, plastic antibodies and natural antibodies. Talanta 279. https://doi.org/10.1016/j.talanta.2024.126543.
Sun, M., Zhang, H., Li, H., Hao, X., Wang, C., Li, L., Yang, Z., Tian, C., 2023. Ag microlabyrinth/nanoparticles coated large-area thin PDMS films as flexible and transparent SERS substrates for in situ detection. Spectrochim. Acta Mol. Biomol. Spectrosc. 303. https://doi.org/10.1016/j.saa.2023.123153.
Sweedan, A.O., Pavan, M.J., Schatz, E., Maaß, H., Tsega, A., Tzin, V., Höflich, K., Mörk, P., Feichtner, T., Bashouti, M.Y., 2024. Evolutionary optimized, monocrystalline gold double wire gratings as a novel SERS sensing platform. Small 20. https://doi.org/10.1002/smll.202311937.
Szekeres, G.P., Kneipp, J., 2019. SERS probing of proteins in gold nanoparticle agglomerates. Front. Chem. 7. https://doi.org/10.3389/fchem.2019.00030.
Tan, Y., Yang, K., Zhang, X., Zhou, Z., Xu, Y., Xie, A., Xue, C., 2023. Stretchable and flexible micro-nano substrates for SERS detection of organic dyes. ACS Omega 8, 14541–14548. https://doi.org/10.1021/acsomega.3c00179.
Tian, L., Jiang, Q., Liu, K.K., Luan, J., Naik, R.R., Singamaneni, S., 2016. Bacterial nanocellulose-based flexible surface enhanced Raman scattering substrate. Adv. Mater. Interfac. 3. https://doi.org/10.1002/admi.201600214.
To, C.Z., Bhunia, A.K., 2019. Three dimensional vero cell-platform for rapid and sensitive screening of Shiga-toxin producing Escherichia coli. Front. Microbiol. 10. https://doi.org/10.3389/fmicb.2019.00949.
Tuckmantel Bido, A., Brolo, A.G., 2023. Digital SERS protocol using Au nanoparticle-based extrinsic Raman labels for the determination of SARS-CoV-2 spike protein in saliva samples. ACS Appl. Nano Mater. 6, 15426–15436. https://doi.org/10.1021/acsanm.3c01979.
Usman, M., Tang, J.W., Li, F., Lai, J.X., Liu, Q.H., Liu, W., Wang, L., 2023. Recent advances in surface enhanced Raman spectroscopy for bacterial pathogen identifications. J. Adv. Res. https://doi.org/10.1016/j.jare.2022.11.010.
Varrone, E., Carnicelli, D., Brigotti, M., 2021. Extracellular vesicles and renal endothelial cells: a fatal attraction in hemolytic uremic syndrome. Am. J. Pathol. https://doi.org/10.1016/j.ajpath.2021.02.011.
Varrone, E., Carnicelli, D., He, X., Grasse, M., Stampfer, K., Huber, S., Kellnerová, S., Tazzari, P.L., Ricci, F., Paterini, P., Ardissino, G., Morabito, S., Orth-Höller, D., Würzner, R., Brigotti, M., 2023. Detection of cleaved Stx2a in the blood of STEC-infected patients. Toxins (Basel) 15. https://doi.org/10.3390/toxins15120690.
Verma, M., Naqvi, T.K., Tripathi, S.K., Kulkarni, M.M., Prasad, N.E., Dwivedi, P.K., 2022a. Plasmonic paper-based flexible SERS biosensor for highly sensitive detection of lactic and uric acid. IEEE Trans. NanoBioscience 21, 294–300. https://doi.org/10.1109/TNB.2021.3124055.
Verma, M., Naqvi, T.K., Tripathi, S.K., Kulkarni, M.M., Prasad, N.E., Dwivedi, P.K., 2022b. Plasmonic paper-based flexible SERS biosensor for highly sensitive detection of lactic and uric acid. IEEE Trans. NanoBioscience 21, 294–300. https://doi.org/10.1109/TNB.2021.3124055.
Wang, Z., Li, M., Wang, W., Fang, M., Sun, Q., Liu, C., 2016. Floating silver film: a flexible surface-enhanced Raman spectroscopy substrate for direct liquid phase detection at gas–liquid interfaces. Nano Res. 9, 1148–1158. https://doi.org/10.1007/s12274-016-1009-x.
Wang, P., Wu, L., Lu, Z., Li, Q., Yin, W., Ding, F., Han, H., 2017. Gecko-inspired nanotentacle surface-enhanced Raman spectroscopy substrate for sampling and reliable detection of pesticide residues in fruits and vegetables. Anal. Chem. 89, 2424–2431. https://doi.org/10.1021/acs.analchem.6b04324.
Wang, B., Park, B., Chen, J., He, X., 2020. Rapid and label-free immunosensing of Shiga toxin subtypes with surface plasmon resonance imaging. Toxins (Basel) 12. https://doi.org/10.3390/toxins12050280.
Wang, L., Jiang, K., Shen, G., 2021. Wearable, implantable, and interventional medical devices based on smart electronic skins. Adv. Mater Technol. https://doi.org/10.1002/admt.202100107.
Wang, J., Liu, S., Meng, Z., Han, X.X., Cai, L., Xu, B., Liu, R., Song, L., He, C., Cheng, Z., Zhao, B., 2023. Flexible SERS biosensor based on core-shell nanotags for sensitive and multiple detection of T1DM biomarkers. Anal. Chem. 95, 14203–14208. https://doi.org/10.1021/acs.analchem.3c01791.
Wang, Y., Wang, Z., Chen, C., Liu, J., Lu, J., Lu, N., 2023. Fabrication of flexible pyramid array as SERS substrate for direct sampling and reproducible detection. Anal. Chem. 95, 14184–14191. https://doi.org/10.1021/acs.analchem.3c01455.
Wang, H., Chen, Y., Yang, Y., Xu, P., Zhang, B., Lu, Y., He, W., Liu, Y., Zhang, J.H., Xiao, X., You, R., 2024. Preparation of cellulose-based flexible SERS and its application for rapid and ultra-sensitive detection of thiram on fruits and vegetables. Int. J. Biol. Macromol. 262. https://doi.org/10.1016/j.ijbiomac.2024.129941.
Wang, K.S., Kuan, T.Y., Chen, Y.C., Chu, Y.J., Chen, J.S., Chen, C.C., Liu, T.Y., 2024. Simultaneous detection of SARS-CoV-2 S1 protein by using flexible electrochemical and Raman enhancing biochip. Biosens. Bioelectron. 249. https://doi.org/10.1016/j.bios.2024.116021.
Wang, Y., Sun, J., Zhou, L., Wu, G., Gong, S., Gao, Z., Wu, J., Ma, C., Zou, Y., Liu, X., Ma, R., Zhang, X., Zhang, Z., Li, Y., 2025. Highly sensitive and interference-free detection of multiple drug molecules in serum using dual-modified SERS substrates combined with AI algorithm analysis. Anal. Chem. https://doi.org/10.1021/acs.analchem.4c06724.
Watanabe-Takahashi, M., Yamasaki, S., Murata, M., Kano, F., Motoyama, J., Yamate, J., Omi, J., Sato, W., Ukai, H., Shimasaki, K., Ikegawa, M., Tamura-Nakano, M., Yanoshita, R., Nishino, Y., Miyazawa, A., Natori, Y., Toyama-Sorimachi, N., Nishikawa, K., 2018. Exosome-associated Shiga toxin 2 is released from cells and causes severe toxicity in mice. Sci. Rep. 8. https://doi.org/10.1038/s41598-018-29128-9.
Willets, K.A., 2009. Surface-enhanced Raman scattering (SERS) for probing internal cellular structure and dynamics. Anal. Bioanal. Chem. https://doi.org/10.1007/s00216-009-2682-3.
Wiriyakun, N., Pankhlueab, K., Boonrungsiman, S., Laocharoensuk, R., 2016. Site-selective controlled dealloying process of gold-silver nanowire array: a simple approach towards long-term stability and sensitivity improvement of SERS substrate. Sci. Rep. 6. https://doi.org/10.1038/srep39115.
Xie, Y., Xu, J., Shao, D., Liu, Y., Qu, X., Hu, S., Dong, B., 2025. SERS-based local field enhancement in biosensing applications. Molecules. https://doi.org/10.3390/molecules30010105.
Xing, T., Qian, Q., Ye, H., Wang, Z., Jin, Y., Zhang, N., Wang, M., Zhou, Y., Gao, X., Wu, L., 2022. Gold nanoparticles with helical surface structure transformed from chiral molecules for SERS-active substrates preparation. Biosens. Bioelectron. 212. https://doi.org/10.1016/j.bios.2022.114430.

Xu, H., Hong, R., Wang, X., Arvizo, R., You, C., Samanta, B., Patra, D., Tuominen, M.T., Rotello, V.M., 2007. Controlled formation of patterned gold films via site-selective deposition of nanoparticles onto polymer-templated surfaces. Adv. Mater. 19, 1383–1386. https://doi.org/10.1002/adma.200700124.

Xu, K., Wang, Z., Tan, C.F., Kang, N., Chen, L., Ren, L., Thian, E.S., Ho, G.W., Ji, R., Hong, M., 2017. Uniaxially stretched flexible surface plasmon resonance film for versatile surface enhanced Raman scattering diagnostics. ACS Appl. Mater. Interfaces 9, 26341–26349. https://doi.org/10.1021/acsami.7b06669.

Xu, J., Cheng, C., Shang, S., Gao, W., Zeng, P., Jiang, S., 2020. Flexible, reusable SERS substrate derived from ZIF-67 by adjusting LUMO and HOMO and its application in identification of bacteria. ACS Appl. Mater. Interfaces 12, 49452–49463. https://doi.org/10.1021/acsami.0c15754.

Xu, Y., Jin, Z., Zhao, Y., 2023. Tunable preparation of SERS-active Au-Ag Janus@Au NPs for label-free staphylococcal enterotoxin C detection. J. Agric. Food Chem. 71, 1224–1233. https://doi.org/10.1021/acs.jafc.2c08147.

Yadav, A., Yadav, A.K., Tarannum, N., Kumar, D., 2024. Paper-based flexible nanoparticle hybrid substrate for qualitative and quantitative analysis of melamine in powder milk by SERS. ACS Omega 9, 2687–2695. https://doi.org/10.1021/acsomega.3c07663.

Yaghoubi, F., Zeinoddini, M., Shoushtari, M., 2023. Detection of shiga-like toxin produced by E. coli O157:H7 based on the LSPR property of gold nanoparticles. J. Appl. Biotechnol. Rep. 10, 1091–1097. https://doi.org/10.30491/jabr.2023.375829.1584.

Yang, Y., Creedon, N., O'Riordan, A., Lovera, P., 2021. Surface enhanced Raman spectroscopy: applications in agriculture and food safety. Photonics 8. https://doi.org/10.3390/photonics8120568.

Yang, Y., Wasiewska, L.A., Burgess, C.M., Duffy, G., Lovera, P., O'Riordan, A., 2022. Detection of stx2 from Shiga toxin-producing Escherichia coli (STEC) by a surface enhanced Raman spectroscopy (SERS) sensor using recycled silicon chips. Sensor. Actuator. B Chem. 373. https://doi.org/10.1016/j.snb.2022.132618.

Yang, J., Zhang, B., Nie, Q., Zheng, R., Lin, P., Wang, C., Lu, Y., Xu, Y., You, R., 2024. Preparation of carboxymethyl cellulose membrane flexible SERS substrate and its application in the detection of metabolites and pH in urine. Int. J. Biol. Macromol. 283. https://doi.org/10.1016/j.ijbiomac.2024.137821.

You, R., Wang, H., Wang, C., Huang, J., Zhu, H., Liu, Y., Zhang, J.H., Liu, J., Yu, X., Lu, Y., 2023a. Bacterial cellulose loaded with silver nanoparticles as a flexible, stable and sensitive SERS-active substrate for detection of the shellfish toxin DTX-1. Food Chem. 427. https://doi.org/10.1016/j.foodchem.2023.136692.

You, R., Wang, H., Wang, C., Huang, J., Zhu, H., Liu, Y., Zhang, J.H., Liu, J., Yu, X., Lu, Y., 2023b. Bacterial cellulose loaded with silver nanoparticles as a flexible, stable and sensitive SERS-active substrate for detection of the shellfish toxin DTX-1. Food Chem. 427. https://doi.org/10.1016/j.foodchem.2023.136692.

Yu, B., Mao, Y., Li, J., Wang, J., Zhou, B., Li, P., Ma, Y., Han, Z., 2022. Hydrophobic expanded graphite-covered support to construct flexible and stable SERS substrate for sensitive determination by paste-sampling from irregular surfaces. Spectrochim. Acta Mol. Biomol. Spectrosc. 282. https://doi.org/10.1016/j.saa.2022.121708.

Yu, H., Guo, D., Zhang, H., Jia, X., Han, L., Xiao, W., 2023. Facile fabrication of flexible AuNPs@CDA SERS substrate for enrichment and detection of thiram pesticide in water. Spectrochim. Acta Mol. Biomol. Spectrosc. 285. https://doi.org/10.1016/j.saa.2022.121930.

Zhang, L., Liu, J., Zhou, G., Zhang, Z., 2020. Controllable in-situ growth of silver nanoparticles on filter paper for flexible and highly sensitive sers sensors for malachite green residue detection. Nanomaterials 10. https://doi.org/10.3390/nano10050826.

Zhang, H., Zhao, N., Li, H., Wang, M., Hao, X., Sun, M., Li, X., Yang, Z., Yu, H., Tian, C., Wang, C., 2022. 3D flexible SERS substrates integrated with a portable Raman analyzer and wireless communication for point-of-care application. ACS Appl. Mater. Interfaces 14, 51253–51264. https://doi.org/10.1021/acsami.2c12201.

Zhang, H., Zhang, Z., Wang, H., Huang, L., Yang, Z., Wang, Y., Li, H., 2023. Versatile flexible SERS substrate for in situ detection of contaminants in water and fruits based on Ag NPs decorated wrinkled PDMS film. Opt. Express 31, 21025. https://doi.org/10.1364/oe.492496.

Zhang, Y., Wang, Y., Liu, A., Liu, S., 2023. Fabrication of flexible SERS substrate based on Au nanostars and PDMS for sensitive detection of Thiram residue in apple juice. Spectrochim. Acta Mol. Biomol. Spectrosc. 297. https://doi.org/10.1016/j.saa.2023.122721.

Zhang, S., Xu, J., He, M., Sun, Z., Li, Y., Ding, L., Wu, L., Liu, X., Du, Z., Jiang, S., 2024. Flexible, scalable and simple-fabricated silver nanorod-decorated bacterial nanocellulose SERS substrates cooperated with portable Raman spectrometer for on-site detection of pesticide residues. Spectrochim. Acta Mol. Biomol. Spectrosc. 315. https://doi.org/10.1016/j.saa.2024.124300.

Zhang, X., Yao, J., Gong, X., Sun, J., Wang, R., Wang, L., Liu, L., Huang, Y., 2024. Paper electrophoretic enrichment-assisted ultrasensitive SERS detection. Food Chem. 434. https://doi.org/10.1016/j.foodchem.2023.137416.

Zhao, H., Zheng, D., Wang, H., Lin, T., Liu, Wei, Wang, X., Lu, W., Liu, Mengjia, Liu, Wenbo, Zhang, Y., Liu, Mengdong, Zhang, P., 2022. In situ collection and rapid detection of pathogenic bacteria using a flexible SERS platform combined with a portable Raman spectrometer. Int. J. Mol. Sci. 23. https://doi.org/10.3390/ijms23137340.

Zhou, X., Li, H., Yu, G., Chen, Y., Wang, Y., Zeng, Z., Chi, L., 2021. A highly-efficient, stable, and flexible Kapton tape-based SERS chip. Mater. Chem. Front. 5, 6471–6475. https://doi.org/10.1039/d1qm00547b.

Zhou, L., Pusey-Nazzaro, L., Ren, G., Chen, L., Liu, L., Zhang, W., Yang, L., Zhou, J., Han, J., 2022. Photoactive control of surface-enhanced Raman scattering with reduced graphene oxide in gas atmosphere. ACS Nano 16, 577–587. https://doi.org/10.1021/acsnano.1c07695.

Zhou, L., Vestri, A., Marchesano, V., Rippa, M., Sagnelli, D., Picazio, G., Fusco, G., Han, J., Zhou, J., Petti, L., 2023a. The label-free detection and identification of SARS-CoV-2 using surface-enhanced Raman spectroscopy and principal component analysis. Biosensors (Basel) 13. https://doi.org/10.3390/bios13121014.

Zhou, L., Vestri, A., Marchesano, V., Rippa, M., Sagnelli, D., Picazio, G., Fusco, G., Han, J., Zhou, J., Petti, L., 2023b. The label-free detection and identification of SARS-CoV-2 using surface-enhanced Raman spectroscopy and principal component analysis. Biosensors (Basel) 13. https://doi.org/10.3390/bios13121014.

Zhou, Y., Zhang, W., Cheng, S., Xing, Y., Wang, J., Yu, F., Wang, R., 2025. Flexible PDMS-SERS platform for culture-free diagnosis of bacterial infections in clinical wound care. Talanta 293. https://doi.org/10.1016/j.talanta.2025.128089.

Zhu, G., Zhu, X., Fan, Q., Wan, X., 2011. Raman spectra of amino acids and their aqueous solutions. Spectrochim. Acta Mol. Biomol. Spectrosc. 78, 1187–1195. https://doi.org/10.1016/j.saa.2010.12.079.

Zhu, A., Ali, S., Xu, Y., Ouyang, Q., Wang, Z., Chen, Q., 2022. SERS-based Au@Ag NPs Solid-phase substrate combined with chemometrics for rapid discrimination of multiple foodborne pathogens. Spectrochim. Acta Mol. Biomol. Spectrosc. 270. https://doi.org/10.1016/j.saa.2021.120814.